Chapter 7

REAL-TIME KINETICS AND HIGH-RESOLUTION MELT CURVES IN SINGLE-MOLECULE DIGITAL LAMP TO DIFFERENTIATE AND STUDY SPECIFIC AND NONSPECIFIC AMPLIFICATION

J.C. Rolando, E. Jue, J. Barlow, and R.F. Ismagilov. 2020. *Nucleic Acids Research.* 48(1):42. doi:10.1093/nar/gkaa099

Abstract

Isothermal amplification assays, such as loop-mediated isothermal amplification (LAMP), show great utility for the development of rapid diagnostics for infectious diseases because they have high sensitivity, pathogen-specificity, and potential for implementation at the point of care. However, elimination of nonspecific amplification remains a key challenge for the optimization of LAMP assays. Here, using chlamydia DNA as a clinically relevant target and high throughput sequencing as an analytical tool, we investigate a potential mechanism of nonspecific amplification. We then develop a real-time digital LAMP (dLAMP) with high-resolution melting temperature (HRM) analysis and use this single-molecule approach to analyze approximately 1.2 million amplification events. We show that single-molecule HRM provides insight into specific and nonspecific amplification in LAMP that are difficult to deduce from bulk measurements. We use real-time dLAMP with HRM to evaluate differences between polymerase enzymes, the impact of assay parameters (e.g., time, rate, or florescence intensity), and the effect background human DNA. By differentiating true and false positives, HRM enables determination of the optimal assay and analysis parameters that leads to the lowest limit of detection (LOD) in a digital isothermal amplification assay.

Introduction

Isothermal methods, such as loop-mediated isothermal amplification (LAMP), are attractive for nucleic acid amplification tests (NAATs) in point-of-care and limited-resource settings (1,2). LAMP in particular shows promise as a NAAT with fewer hardware requirements compared with PCR (3). Despite advancements, the ability to optimize LAMP NAATs for a specific target sequence and primer set (specific to a target organism) remains constrained by a limited understanding of how amplification is affected by myriad factors, including polymerase choice, primer design, temperature, time, and ion concentrations. In particular, addressing nonspecific amplification remains a core problem as it constrains an assay's limit of detection (LOD). In reactions containing template target molecules, both specific and nonspecific amplification reactions may occur. Unlike PCR, LAMP lacks a temperature-gating mechanism, so nonspecific reactions consume reagents and compete with specific amplification impacting its kinetics. The presence of nonspecific amplicons therefore adversely impacts both the assay's analytical sensitivity (the fewest template molecules that can be detected) and its analytical specificity (ability to detect the target template in the presence of competing reactions). Classifying reactions as either specific or nonspecific amplification would therefore be invaluable both during assay optimization and assay deployment in clinical diagnostics.

Substantial research is focused on using isothermal amplification chemistries for diagnosis of infectious disease. For example, chlamydia (caused by the pathogen *Chlamydia trachomatis,* CT) is the most common sexually transmitted infection worldwide, with more than 110 million cases reported annually (4). Diagnosis of CT infections is challenged by a lack of standard symptoms (many infections are asymptomatic) (5) and the presence of mixed flora (particularly in the female reproductive tract) (6). Thus, rapid NAATs with high sensitivity and specificity are critically needed, especially NAATs that can deal with the high levels of host or background DNA likely to be present in clinical samples such as urine samples and swabs (7,8).

Optimizing LAMP for CT and other infectious pathogens requires addressing and reducing nonspecific amplification or a method for separating nonspecific reactions from specific amplification. Reactions run in bulk (i.e., in a tube) in the absence of template can be informative to provide information on performance of nonspecific amplification. Another method to identify nonspecific amplification includes mathematical modeling in conjunction with electrophoresis to distinguish between nonspecific and specific banding patterns(9). However, in the presence of template, although specific and nonspecific reactions occur simultaneously, they cannot be monitored simultaneously. Thus, bulk reactions have three important limitations with regard to assay optimization: (i) differences in the kinetics of specific and nonspecific reactions cannot be separated; (ii) rare but significant events, such as early but infrequent nonspecific amplification, cannot be easily characterized; and (iii) testing the full design space requires many hundreds of replicates to obtain statistically significant data. To improve an assay's analytical specificity and sensitivity, one strategy is to eliminate the detection of nonspecific amplification. In bulk LAMP experiments, nonspecific amplification can be excluded from detection by using probes, beacons, FRET, or reporter-quencher schemes that show only specific amplification of the target (10-19). Although these methods improve the assay, they do not capture nonspecific reactions and thus cannot give insights into the origin of nonspecific amplification or the conditions that led to nonspecific amplicons. Moreover, probes and beacons do not eliminate nonspecific amplification; nonspecific amplification still competes for reagents and can limit the extent of the signal generated by specific amplification events (20). Hence, it is highly desirable to distinguish specific from nonspecific amplification.

In this study, we combined sequencing and digital single-molecule LAMP (dLAMP) with high-resolution melting temperature (HRM) to probe the fundamental mechanics of amplification reactions. We used dLAMP to extract real-time kinetic information to identify the digital threshold data-processing parameters that minimize nonspecific amplification events and elucidate how an interfering molecule impacts amplification. Digital single-molecule methods separating individual amplification events into discrete compartments, eliminating interference among individual amplification events (21,22). Furthermore, digital experiments consist of thousands of reactions that run in parallel and thus provide valuable

statistical information (21-23). We used real-time imaging to monitor the kinetics of 20,000 dLAMP reactions per experiment and observe ~ 1.2 x 10^6 reactions in total. We hypothesized that high-resolution melting analysis (HRM) could be a tool for separating specific from nonspecific amplification events and for identifying the optimal digital threshold data-processing parameters to distinguish specific and nonspecific amplification events (even when an assay is deployed without HRM). To test this hypothesis, we used a dLAMP assay with CT DNA as the target (combined with sequencing to identify the products of bulk reactions) to analyze both specific and nonspecific amplification under conditions that include clinically relevant concentrations of background human DNA.

Materials and Methods

LAMP reagents

IsoAmp I (#B0537S), IsoAmp II (#B0374S), $MgSO_4$ (#B1003S), deoxynucleotide solution (#N0447S), Bovine Serum Albumen (BSA, #B9000S0), *Bst* 2.0 (8,000 U/mL, #M0537S), and *Bst* 3.0 (8,000 U/mL, #M0374S) were purchased from New England Biolabs (Ipswich, MA, USA). Ambion RNase Cocktail (#AM2286), Ambion nuclease-free water (#AM9932), Invitrogen SYTO 9 (S34854), and Invitrogen ROX Reference Dye (#12223012) were purchased from Thermo Fisher Scientific (Waltham, MA, USA). We found it important to use SYTO 9 dilutions within one week of preparation.

Primers sequences were targeted against the *Chlamydia trachomatis* 23S ribosomal gene using Primer Explorer V5 (Eiken Chemical, Tokyo, Japan) and checked in SnapGene (GSL Biotech, Chicago, IL, USA) to ensure the sequences were in a mutation-free region from the available Genebank sequences of CT. Primers were purchased from Integrated DNA Technologies (San Diego, CA, USA) and suspended in nuclease-free water. For all experiments, the final concentrations of primers were 1.6 µM FIP/BIP, 0.2 µM FOP/BOP, and 0.4 µM LoopF/LoopB. Primer sequences are listed in Supplementary Materials and Methods.

LAMP experiments using *Bst* 2.0 were amplified at 68 °C in nuclease-free water, with final concentrations of: 1x IsoAmp I Buffer, 7mM total $MgSO_4$ (5 mM additional), 1.4 mM each dNTP, 1.25 uM ROX Reference Dye, 1 mg/mL BSA, 320 U/mL *Bst* 2.0, 1x Ambion RNase Cocktail, and 2 uM SYTO 9.

LAMP experiments using *Bst* 3.0 were amplified at 69 °C in nuclease-free water, with final concentrations of: 1x IsoAmp II Buffer, 8mM total $MgSO_4$ (6 mM additional), 1.4 mM each dNTP, 1.25 uM ROX Reference Dye, 1 mg/mL BSA, 320 U/mL *Bst* 2.0, 1x Ambion RNase Cocktail, and 2 uM SYTO 9.

For both enzymes, after 90 min of amplification, reactions were ramped to 95°C at maximum output and held for 30 sec to inactivate the enzymes. Chips were cooling to 55°C and the melt performed at a ramp rate of 1 °C per image from 55–90 °C, and a ramp rate of 0.5 °C per image from 90–95 °C.

Extraction of spiked Chlamydia trachomatis *(CT) from a relevant clinical matrix*

A frozen stock of live CT (D-UW3, Z054, Zeptometrix, Buffalo, NY, USA) was re-suspended in pre-warmed (37 °C) SPG buffer (219 mM sucrose, 3.7 mM KH2PO4, 8.5 mM NA2HPO4, and 4.9 mM L-glutamate) to 1E8 IFU/mL. It was then diluted 10-fold into a freshly donated urine sample to $1x10^7$ IFU/mL. Urine from a healthy human donor (>18 years of age) was acquired and used in accordance with approved Caltech Institutional Review Board (IRB) protocol 15-0566. Written informed consent was obtained from all participants, donations were never tied to personal identifiers, and all research was performed in accordance with relevant institutional biosafety regulations. A 250 µL aliquot from this CT-spiked urine sample was then extracted following the ZR Viral DNA/RNA Kit protocol (#D7020, Zymo Research, Irvine, CA, USA). Briefly, 250 µL of CT-spiked urine was mixed with 250 µL DNA/RNA shield and 1000 µL DNA/RNA Viral Buffer. 1500 µL (750 µL x 2) was added to the column and centrifuged at 16,000 xg for 1 min. Then, 500 µL Viral Wash buffer was added to the column and centrifuged at 16,000 xg for 2 min. Lastly, 60 µL

DNAse/RNAse-free water was added directly to the column and centrifuged at 16,000 xg for 30 s. The eluent was treated by adding 2.5 µL Ambion RNAse Cocktail (#AM2286, Thermo Fisher Scientific) to 47.5 µL template. Stocks were prepared in 0.5x TE buffer and dilutions quantified using the QX200 droplet digital PCR system (Bio-Rad Laboratories, Hercules, CA, USA), outer primers at 500 nM each, and 1x EvaGreen Supermix (Bio-Rad).

Fabrication of thermoelectric unit and mount

A Thermoelectric Module (VT-127-1.4-1.5-72), Thermister (MP-3022), Controller (TC-720), and 12V Power Supply (PS-12-8.4; TE Tech, Traverse City, MI, USA) were wired according to the manufacturer's instructions.

While the Peltier can be used out of the box, we manufactured a heat plate and sink to improve the efficiency in the cooling mode. Instructions for fabrication can be found in the Supplementary Materials and Methods, "Fabrication of thermoelectric unit mount." The ability of the embedded thermocouple to accurately assess temperature of the aluminum block was verified with an independent K-type mini-thermcouple read through a General IRT659K [IR] Thermometer.

Shearing of genomic DNA

Human genomic DNA from buffy coat leukocytes (Roche (via Sigma Aldrich), Reference 11691112001) was fragmented using a Covaris Focused Ultrasonicator M220 (Woburn, MA, USA) equipped with 130 µL microTUBE AFA Fiber Snap-Cap at 50W peak power, 5% duty factor, 200 cycles per burst, for 80 sec. Fragment concentration was determined using a Qbit 3 Fluorimiter (Thermo Fisher, Ref # Q33216) with dsDNA HS assay kit (ThermoFisher, Ref #Q32851), and mean fragment size determined as 365 bp using an Agilent 4200 TapeStation (#G2991AA, Agilent, Santa Clara, CA, USA) and High Sensitivity D5000 ScreenTape (#5067-5592) with ladder (#5190-7747), and D100

ScreenTape (#5067-5584) with High Sensitivity D1000 Reagents (#5067-5585). Dilutions were prepared with a final concentration of 0.5x TE buffer.

Microfluidic chips

Microfluidic chips for dLAMP (#A26316; Applied Biosystems, Foster City, CA, USA) were loaded as we have described previously (23) at a concentration where ~40% of partitions would fluoresce (corresponding to the Poisson maximum single template per partition loading of 660 cp/µL). We estimated the volume of each partition to be 750 pL. To achieve this concentration of template molecules, we diluted template stocks from storage in 0.5x TE to ~0.03x TE for all experiments. Genomic DNA (gDNA) stocks, also stored in 0.5x TE, were diluted to a final concentration of 0.077x. Thus, the total final concentration of TE for all experiments of was approximately 0.1081x TE buffer.

Microscopy data collection

Data were collected in 30-sec intervals using a DMI-6000B microscope (Leica, Buffalo Grove, IL, USA) equipped with a 1.25x 0.04NA HCX PL FLUOTAR Objective and 0.55x coupler (Leica C-mount 11541544). The response from SYTO 9 was recorded using a 1.5-sec exposure through an L5 (GFP) Nomarski prism, while the ROX Reference Dye was collected using a 1-sec exposure through a Texas Red prism. Images were collected using a Hamamatsu ORCA-ER CCD camera (Hamamatsu Photonics K.K., Hamamatsu City, Japan) at 100 gain. Temperature was recoded using the built-in features of the TC-720 Controller in approximately one second intervals and correlated to the images via image metadata.

In these experiments, we chose to use a microscope, instead of the custom real-time amplification instrument we used previously (23,24), because the microscope has superior optical properties (greater pixels per partition and lower exposure time requirements) to access higher temporal resolution and enhanced kinetic measurements.

MATLAB script processing

The MATLAB script processes a .txt file with temperature-time data generated from the TE Tech Controller and a TIF stack containing 2-channel images of the LAMP and melt curve from the LEICA microscope. Partitions are identified using a custom iterative thresholding algorithm, and labels are propagated throughout the TIF stack using a custom labeling algorithm. Average well intensity is tracked over time to generate LAMP curves and plotted against temperature to generate the melt curves. Complete details of the script are in the Supplementary Materials and Methods, "MATLAB script."

Bulk LAMP reactions were conducted in 10 µL volumes within a well plate on a CFX96 Real-time Thermocycler (Bio-Rad) at buffer conditions and temperatures matching the dLAMP reactions.

Enzymatic digestions of bulk LAMP products were conducted using CAC8I (Ref #R0579S), Hpy166II (Ref #R0616S), ACCI (Ref #R0161S), AciI (Ref #SR0551S), MseI (Ref #R0525S), and HpyCH4III (Ref #R0618S) purchased from New England Biolabs and were conducted in 50 µl reaction volumes containing 1 µL enzyme, 1 µg DNA, in 1 x Cut Smart Buffer, and incubated for 1 h at 37 °C. Samples were inactivated for 1 h at 80 °C and diluted to 1 ng/µL (~1:300) to run on an Agilent 4200 TapeStation using High Sensitivity D5000 ScreenTape (#5067-5592) with ladder (#5190-7747), and D100 ScreenTape (#5067-5584) with High Sensitivity D1000 Reagents (#5067-5585).

Library preparation and sequencing

300-500 ng of amplified DNA products were fragmented to the average size of 200 bp with Qsonica Q800R sonicator (power: 20%; pulse: 15 sec on/15 sec off; sonication time: 12 min), and libraries were constructed using NEBNext Ultra™ II DNA Library Prep Kit (NEB, #E7645) following manufacturer's instructions. Briefly, fragmented DNA was end-repaired,

dA tailed, and ligated to NEBNext hairpin adaptors (NEB, #E7335). After ligation, adapters were converted to the ”Y” shape by treating with USER enzyme and DNA fragments were size selected using Agencourt AMPure XP beads (Beckman Coulter, Ref #A63880) to generate fragment sizes between 250 and 350 bp. Adaptor-ligated DNA was PCR amplified with 5 cycles followed by AMPure XP bead clean up. Libraries were quantified with Qubit dsDNA HS Kit (ThermoFisher Scientific, #Q32854), and the size distribution was confirmed with High Sensitivity DNA Kit for Bioanalyzer (Agilent Technologies, #5067). Libraries were sequenced on Illumina HiSeq2500 in single-read mode with the read length of 50 nt to the sequencing depth of 10 million reads per sample, following manufacturer's instructions. Base calls were performed with RTA 1.18.64 followed by conversion to FASTQ with bcl2fastq 1.8.4.

Sequencing analysis

Raw FASTQ files were first analyzed with FastQC v0.11.8. Overrepresented sequences were compared with input primer sequences to find reads consisting of potential products from the LAMP reactions. To verify that all adjoining products were accounted for, the FASTQ files were aligned to the predicted products using Bowtie2 v2.3.4.3 with global very-sensitive settings. Unaligned reads were checked for any remaining possible amplification products. All regions consisting of sequences from multiple primers were tallied by counting the reads with a substring of n=11 from the end of each primer. One adjoining region between primers contained a random insertion of nucleotides and was analyzed by first extracting all reads containing the primer before and after the random nucleotides. The length and sequence distribution of random inserts was then analyzed from the extracted reads.

Results and Discussion

Bulk LAMP studies reveal nonspecific products with high melting temperature (Tm)

We first wished to test whether melting temperature (Tm) could be used to separate specific and nonspecific amplification in a LAMP assay run in bulk. To start, we selected a concentration near the LOD where we might observe both specific and nonspecific amplification. We used extracted CT genomic DNA in the presence of two commercially available polymerases, *Bst* 2.0 and *Bst* 3.0, with CT 23S as the amplification target. At target molecule concentrations of 10 copies per µL (cp/µL), amplification using *Bst* 2.0 polymerase began between 10-11 min (**Figure 1.1A**) and had uniform Tm (**Figure 1.1B**). Amplification using *Bst* 3.0 polymerase (**Figure 1.1C**), also yielded amplification from 10-11 min; however, we also observed a nonspecific amplification at 15 min, defined as having a different Tm than the specific amplification events (**Figure 1.1D**). This indicated *Bst* 3.0 could be a useful model for studying nonspecific amplification. We observed that early amplifying products corresponded to specific amplification events, and the later products corresponded to nonspecific amplification, supporting our prediction that we could use Tm as a proxy for sequence identity, as is common with PCR, and has been used previously in LAMP (25-29).

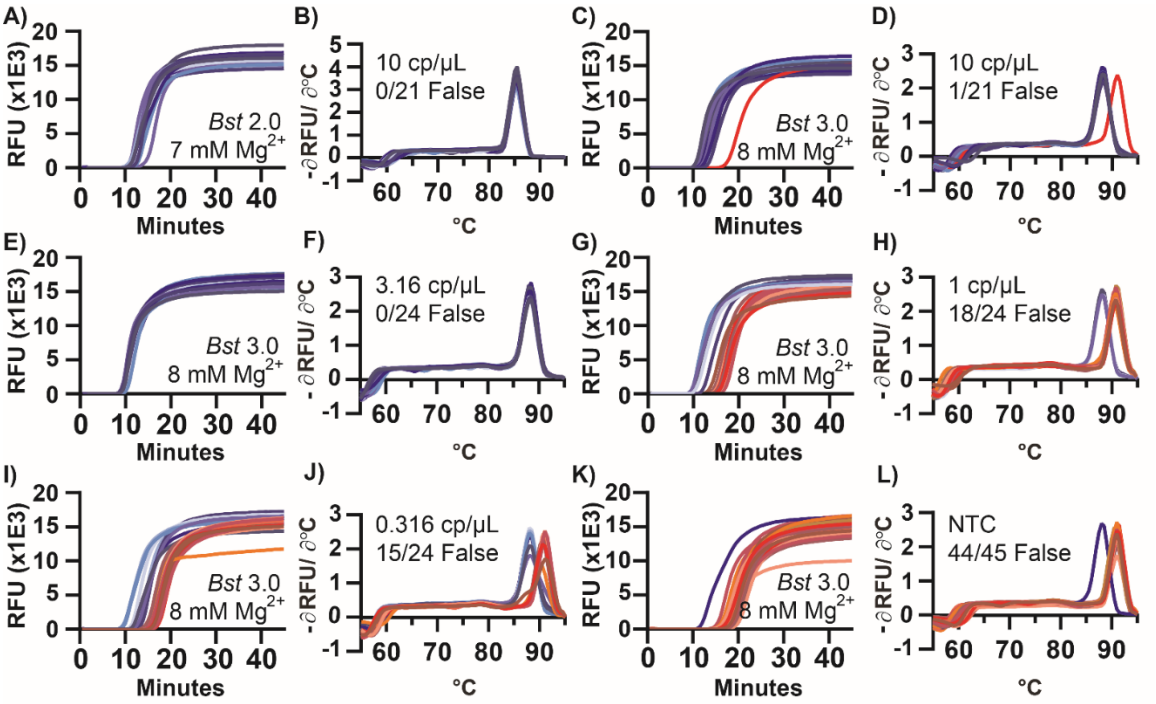

Figure 1.1: Amplification and melting temperature (Tm) curves of *Chlamydia trachomatis* in a bulk reaction show nonspecific amplification products with high Tm.

Plots of fluorescence as a function of time during a LAMP reaction (A,C,E,G,I,K) and the derivative plot of fluorescence as a function of temperature for the corresponding melting curves (B,D,F,H,I,J). Reactions using *Bst* 2.0 at 10 copies per microliter (cp/µL) (A,B), and using *Bst 3.0* at 10 cp/µL (C,D), 3.16 cp/µL (E,F), 1 cp/µL (G,H), 0.316 cp/µL (I,J), and without template (K,L). Reactions of specific amplification are different shades of blue; nonspecific amplification is different shades of red. The number of false-positive reactions is reported within each panel as $N/N_{reaction}$ False. N_{Total} for all conditions = 159 reactions.

Using *Bst* 3.0 at low concentrations of target is a useful system to study nonspecific amplification. To investigate the role of the concentration of the target on the incidence of nonspecific amplification, we performed half-log dilutions of template from 10 to 0.316 cp/µL. At 3.16 cp/µL (**Figure 1.1E-F**), only specific amplification occurred (24 replicate

wells/plate). However, once template concentrations reached 1 cp/µL (**Figure 1.1G-H**), nonspecific amplification occurred with greater frequency than specific amplification (18 of the 24 replicates generated false positives). Similarly, for 0.316 cp/µL (**Figure 1.1I-J**) 15 of the 24 replicates generated false positives. We next ran the same assay in the absence of template (no-template control, NTC) (**Figure 1.1K-L**). Even though we did not expect amplification, we observed all reactions amplified. 44 of 45 replicates amplified at a Tm of 91 °C, consistent with the Tm of nonspecific amplification in the presence of template. Although it is possible for a reaction to generate multiple different nonspecific amplification products, even ones with Tm matching to the specific products, the single amplicon observed at 88 °C in the NTC was a contaminant that appeared to have the same sequence as the specific products (**Figure 1.2A [well F8]**). In general, when the specific target was present, it amplified sooner and outcompeted the nonspecific amplification, thereby reducing the number of observations of nonspecific amplification. To determine if the nonspecific amplification was inherent to the polymerase or a consequence of buffer selection, we conducted additional studies using both Bst polymerases (**Supplementary Figure 1.11 and Table 1-1**).

To better understand nonspecific amplification in LAMP, we investigated the sequence identity of the nonspecific products with high Tm using sequencing and gel analysis and compared them with the specific products. The Tm of specific amplification differed between the two polymerases tested. Specific amplification for *Bst* 2.0 had a Tm of 85.5 °C, whereas specific amplification using *Bst* 3.0 had a Tm of 88 °C, and demonstrated nonspecific amplification at Tm of 91 °C. The nonspecific amplification had identical Tm to amplification in absence of template (**Figure 1.1K,L**). Despite the specific amplification products of *Bst* 2.0 and *Bst* 3.0 producing similar gel banding patterns (**Figure 1.3**) and the same sequencing results (see **Figure 1.2B**), they had different Tm (**Figure 1.1B,D** respectively). We determined the difference in Tm was due to differences in buffer conditions (**Supplementary Figure 1.11 and Table 1-1**).

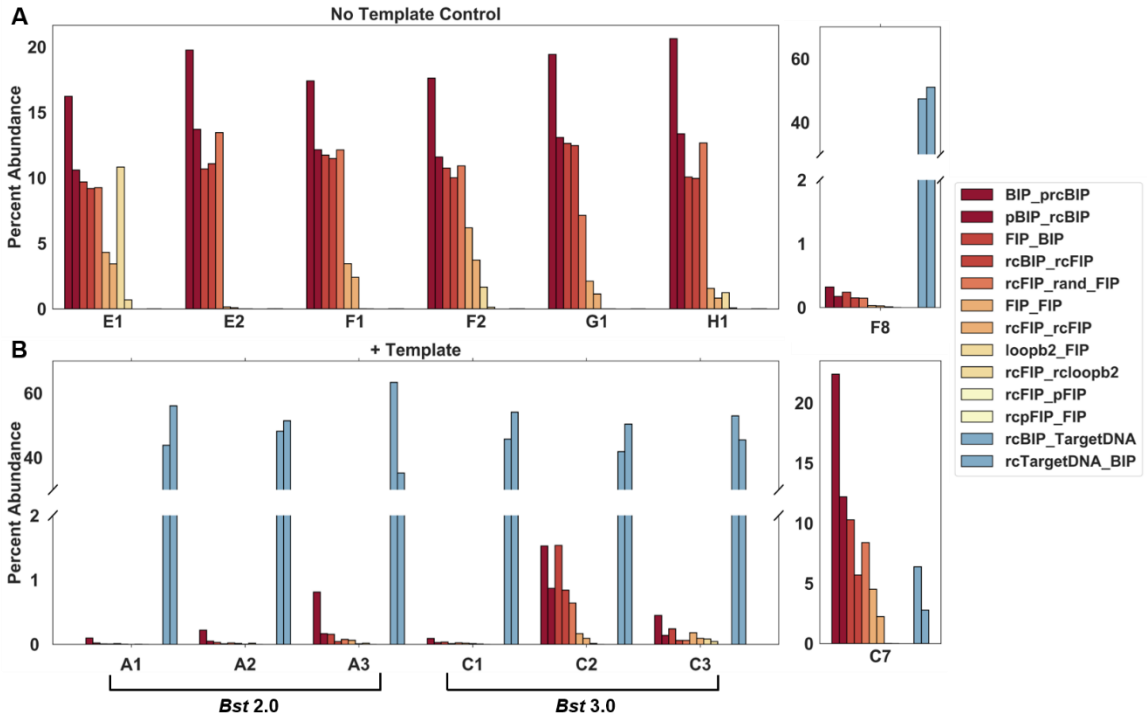

Figure 1.2: Quantification of junctions using next-generation sequencing of select *Chlamydia trachomatis* amplification products from bulk reactions. Nonspecific amplification from the no-template control using *Bst* 3.0 (A), including amplification of a specific target contamination (well F8) corresponding to **Figure 1.1**K,L. Amplification in the presence of 10 cp/µL template (B), using *Bst* 2.0 (wells A1-A3) corresponding to **Figure 1.1A,B**, and *Bst* 3.0 (wells C1-C3) corresponding to **Figure 1.1C,D**. Nonspecific amplification in the presence of 10 cp/µL template and *Bst* 3.0 (well C7) corresponding to **Figure 1.1C,D**. For a complete list of abbreviations used in this figure, see Supplementary **Table 1-2**.

In all bulk reactions, we observed nonspecific products with high Tm. This was surprising because in PCR, primer dimers have low Tm; moreover, in previous demonstrations of LAMP, Tm was lower for nonspecific compared with specific products (27). Thus, we investigated the sequence identity of the nonspecific product with high Tm. We ran the LAMP products on a gel and observed that the characteristic pattern of the specific

amplification products differed substantially from the banding pattern seen in the high-Tm nonspecific products (**Figure 1.3**). Interestingly, the high-Tm nonspecific product had a ladder pattern resembling that of specific LAMP products.

To determine the identity of the high-Tm nonspecific products, we performed next generation sequencing (NGS). We observed that the nonspecific products lacked the corresponding target sequence and identified the product as a mixture of full-length FIP, BIP, and their complements, as well as fragments of BIP (**Figure 1.2A**).

To confirm the sequence identity of the amplicon, we targeted the FIP and BIP regions using several restriction endonucleases. Digestion of the specific and nonspecific products resulted in different banding patterns than the undigested samples, and was consistent with the presence of both FIP and BIP endonuclease recognition sites within the sequence (**Supplementary Figure 1.12**). Specific amplification products were 47% GC; nonspecific amplification products were 53% GC.

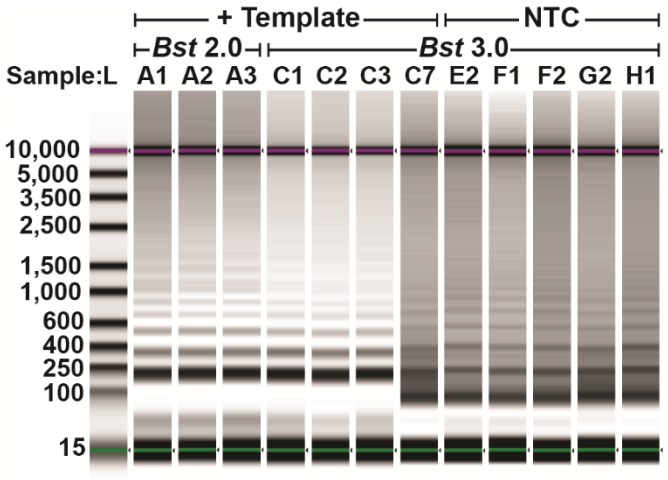

Figure 1.3: Composite image of select *Chlamydia trachomatis* amplification products from a bulk reaction.

Products were collected using D5000 tape on Agilent TapeStation. Amplification in the presence of 10 cp/µL template using *Bst* 2.0 (lanes A1-A3) corresponding to

Figure 1.1A,B, and *Bst* 3.0 (lanes C1-C3, C7) corresponding to **Figure 1.1C,D**. Nonspecific amplification in the no-template control (NTC; lanes E2-H1) corresponds to **Figure 1.1K,L**. Contrast was determined using the automatic "scale to sample" feature in the Agilent TapeStation analysis software.

A proposed mechanism for formation of nonspecific product

We hypothesize a mechanism for the formation of the nonspecific product with high Tm originating as a consequence of interactions of the *Bst* polymerase and LAMP inner primers. Other potential mechanisms include LIMA (30) and UIMA (31), but are inconsistent with our sequencing results, which observe nearly equal reads of the forward and reverse strand as measured by counting the complementary sequences between each junction. Our proposed mechanism requires properties that have been observed with *Bst* enzymes: a strand-displacing polymerase lacking 3'-5' exonuclease activity—common to polymerases from thermophilic bacteria (32,33), template switching ability to allow synthesis across a discontinuous template (33), terminal transferase activity, or the ability to perform non-templated synthesis (32,34,35). Briefly, the nonspecific product likely arises from extension of a low probability homo-dimerization of the Backward Inner Primer (BIP), followed by elongation across a discontinuous junction ("template switching") to form a double-stranded product incorporating Forward Inner Primer (FIP). Through breathing of the molecule, the 3' of one strand may form a second hairpin and amplify. Some of these amplification events incorporate several random nucleotides via terminal nucleotidyl transferase activity resulting in a pool of hairpins with 3' randomers. Sequences with complementary randomers are selected *in vitro* to amplify. The double-stranded product of this amplification can, through intramolecular hydrogen bonding, form two dumbbell-like structures and amplify in a fashion similar to the standard LAMP mechanism, but primed by BIP. Repetitive cycles of self-priming and hairpin priming by BIP result in numerous sequences with complementarity and the possibility of multiple replication loci within a single molecule. This process can give rise to very long amplicons, and even a branched, mesh-like network from the multimeric

sequences annealing to their neighbors or in a self-complementary fashion. A simplified version of this mechanism, annotated with sequencing data, can be found in **Supplementary Figure 1.13**.

In more detail, a potential mechanism of formation of nonspecific products is as follows: Initially, a double-stranded amplicon is generated by homo-dimerization of BIP, and 3' extension of the homodimer to produce a partial reverse complement of BIP (prcBIP) (**Figure 1.4-1**). *Bst* polymerase is highly prone to mismatched extension (36), and the two base pairs of CG provide a sufficient anchoring in the 3' to start elongation. Multiple Primer Analyzer (ThermoFisher) does not identify the BIP homodimer, unless maximum sensitivity is used. Alternatively, BIP-prcBIP product may arise from a single stranded BIP-hairpin, as has been observed by others (37), although UNAfold (IDT) does not predict the formation of the hairpin for this primer. These structures may not need to be abundant at equilibrium, but as long as they are extended by the polymerase, the product will be stabilized and will accumulate.

Upon accumulation of the BIP-prcBIP construct, the reverse complement of FIP (rcFIP) is incorporated by template switching (**Figure 1.4-2**). The 3' of FIP is within spatial proximity of the homo-BIP sequence due to microhomology of to 5' end of the double-stranded sequence coupled with rapid breathing of two base pairs of TA. This allows temporary insertion and hybridization of FIP with the double-stranded BIP-prcBIP sequence (**Figure 1.4-3**). When the polymerase is also in proximity of this reaction, FIP slips out of the junction, and the polymerase elongates across the 3' discontinuous junction (33,35) templated by FIP (**Figure 1.4-4**). We confirmed the interaction of FIP and BIP produced the high-Tm nonspecific amplification, and that elimination of 3' microhomology could significantly reduce high-Tm nonspecific amplification (**Supplementary Figure 1.14-16, Table 1-3, Table 1-4**). After elongation, the FIP which has served as template, is poised to prime in the opposite direction (**Figure 1.4-5**). This either displaces the initial BIP mispairing (BIP*) or opens the hairpin, resulting in a double-stranded BIP-prcBIP-FIP product (**Figure 1.4-6**). This three-part junction is observed as a complete product in NGS data. Breathing of double-stranded BIP-prcBIP-FIP is prone to formation of an intramolecular self-priming hairpin of

rcBIP-pBIP (**Figure 1.4-7**). Elongation of the 3' hairpin results in a double-stranded FIP-pBIP-rcBIP-rcFIP hairpin (**Figure 1.4-8**) and displacement of a BIP-prcBIP-rcFIP hairpin (**Figure 1.4-9**), which may be primed by FIP to restart this cycle (**Figure 1.4-10**). With each amplification, and re-prime by FIP, a single product is generated. This process of hairpin accumulation would cause the linear "rinsing" baseline observed by other researchers (37).

Within this pool of linear amplifying products, the *Bst* enzyme will randomly incorporate additional nucleotides at the 3' end of FIP-pBIP-rcBIP-rcFIP via terminal transferase activity (**Figure 1.4-11**). Our sequencing methods are unable to observe a FIP-randomer hairpin because adapter ligation requires double-stranded products. This pool of hairpins with random sequences will accumulate until LAMP selects for sequences that amplify by sharing complementary 3' "toe holds" (**Figure 1.4-12**). Much like *in vitro* evolution, those sequences with the highest probability of amplification are selected (32). The lack of a thermal gating mechanism in LAMP and lack of 3'–5' exonuclease activity makes the amplification reaction especially prone to *in vitro* evolution of self-amplifying products. When considered in this light, it is unsurprising that nonspecific amplification could arise from mechanisms similar to the specific products. Within a given bulk reaction, variation in randomer sequence length and identity was low. However, between different samples, randomer sequences of multiple lengths and identities were observed. These two results further suggest that in bulk reactions amplification occurs from one or a few sequences (**Supplementary Table 1-5, Table 1-6, Table 1-7**).

Elongation from the randomer overhang results in a double-stranded products, leading to dumbbell structures, and LAMP-like amplification. First, elongation of hairpins with complementary randomer toe holds produces a dimer of FIP-BIP-prcBIP-rcFIP coupled through the randomer (**Figure 1.4-13**). Breathing of the molecule can result in formation of intramolecular hairpins, and eventual disassociation into two separate self-priming, dumbbell shaped hairpins (**Figure 1.4-15 and -16**). The products of elongation from self-priming amplification doubles the amount of dsDNA present and forms sequences with internal hairpins capable of priming by BIP (**Figure 1.4-17**). Elongation from BIP priming creates a new double-stranded product and reveals a self-priming 3' hairpin of the original strand

(**Figure 1.4-18**), which upon elongation, displaces the sequence primed by BIP (**Figure 1.4-19**) while transforming the trimer of FIP-BIP-prcBIP-rcFIP to a pentamer (more than tripling the amount of ds products from structures 15 and 16). The pentamer still contains an rcBIP hairpin, and may amplify in a functionally similar method as previously (**Figure 1.4-17**). The displaced product **Figure 1.4-19** is similar to **Figure 1.4-16** but missing 5'-FIP. However, much as with **Figure 1.4-16**, this products is self-priming and produces a structure with an internal rcBIP hairpin (**Figure 1.4-20**). A second priming of the hairpin by BIP of the rcBIP-pBIP hairpin and subsequent elongation, creates a new double-stranded product and reveals a self-priming 3' hairpin of the original strand (**Figure 1.4-21**). As previously, upon elongation, the sequence primed by BIP is displaced (**Figure 1.4-22**). Simultaneously, the self-priming event turns the FIP-BIP-prcBIP trimer to a pentamer, which may continue to be amplified by BIP. The released sequence (**Figure 1.4-22**) is again self-priming, and its product is equivalent to **Figure 1.4-20** to restarts the cycle. Further, amplified hairpins may, in addition to BIP priming of the hairpin, duplicate through self-priming by breathing and formation of a 3' rcBIP-pBIP hairpin (**Figure 1.4-23**).

The products of these reactions are capable of forming a branched, mesh-like network resulting in the observed high temperature melting. Products may experience random internal priming by through hairpin formation (e.g. **Figure 1.4-13,-17,-20**), or 3' self-priming (**Figure 1.4-23**). Consequently, multiple replication loci may exist within a single strand, and products may have internal stem loop structures (**Figure 1.4-24**). Furthermore, in addition to intramolecular bonding, the highly repetitive nature of these products allows for melting of fragment, which reanneals to self in a different conformation, or a neighboring strand.

Though the initial steps of generating a double-stranded hairpin will be unique to our particular primer set, once a seed is generated, the processes of template switching and terminal transferase activity should be a general phenomenon associated with nonspecific amplification of thermophilic polymerase resulting in exponential amplification. As evidenced, when the mechanism of seed formation is disrupted through elimination of the microhomology, amplicons with high Tm still occur, albeit with lower frequency and delayed occurrence (**Supplementary Figure 1.14-16, Table 1-3, Table 1-4**). Template

switching and non-template synthesis are 100x slower than template extension (33). However, once the self-amplifying products are selected, the reaction follows standard exponential LAMP enrichment. Thus, accumulation of a sufficient pool of randomers may take time, but still result in a delayed bulk exponential amplification event. Furthermore, should a hairpin with attached randomer form, it is possible that the rising baseline, attributed to hairpin formation (37), may also be *in vitro* selection of the products, leading to and resulting in spontaneous exponential amplification.

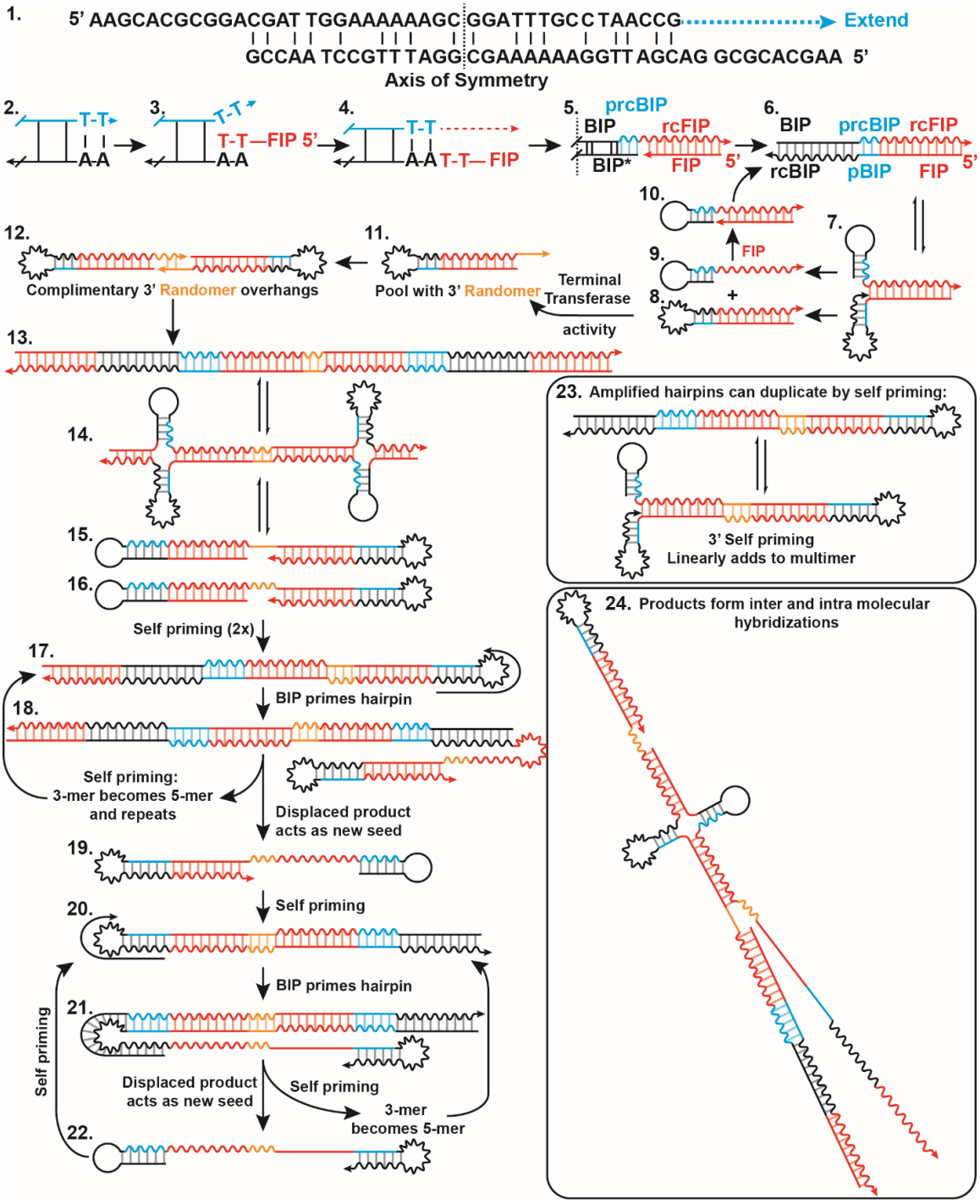

Figure 1.4: Illustration of a mechanism for formation of nonspecific amplification products in LAMP reactions.

Putative structures and intermediates are labeled with numbers. Forward sequences are illustrated as a straight line, and the reverse compliment as a wavy line of

matching color. Abbreviations used in this figure: BIP, Backward Inner Primer; rcBIP, Reverse compliment of BIP; FIP, Forward Inner Primer; rc FIP, Reverse Compliment of FIP; prcFIP, Partial Reverse Compliment of FIP.

Melting temperature differentiates specific and nonspecific reactions in dLAMP

To study specific and nonspecific amplification events at the digital single-molecule level, we developed a new approach that enabled HRM analysis (obtaining "melt curves") to be performed on each partition. We used a commercially available microfluidic chip with 20,000 partitions and a previously published open-source dLAMP method accessible to most standard laboratories (23) with the following improvements: incorporation of an off-the-shelf thermoelectric unit to both heat and cool the chips, and an enhanced MATLAB script to allow for multicolor tracking. We used the temperature-independent fluorophore ROX to track each partition's location and the dsDNA intercalating fluorophore SYTO 9 to follow amplification and hybridization status. This two-channel approach is required to follow a partition through both amplification and the entirety of the HRM when fluorescence from SYTO 9 is lost.

As an illustration of the capabilities of our approach, we first used real-time dLAMP to study the kinetic parameters of individual reactions, and we used Tm to classify reaction outcome (**Figure 1.5**). Using real-time dLAMP, we followed individual partitions as they amplified as a function of time (**Figure 1.5A**) and then by temperature as they went through HRM (**Figure 1.5B**). Real-time imaging of individual partitions enables us to reconstruct the standard amplification curves of intensity for each partition as a function of time (**Figure 1.5C**), and plotting the fluorescence intensity as a function of temperature yields an HRM trace (**Figure 1.5D**); the negative derivative plot (**Figure 1.5E**) of this melt trace is the standard melt curve. Analogous to bulk measurements, the standard melt curve is used to classify reactions as specific or nonspecific. We used these classifications to identify important patterns in the kinetics of each type of amplification (**Figure 1.5F-H**).

We next used real-time dLAMP with HRM to determine whether differences in time to positive (TTP) were due to a difference in amplification initiation or in rate. We expect this information would be valuable for elucidating whether the molecules that lead to bulk amplification are the ones that are first to initiate or the ones that initiate with the fastest rates. We found that TTP can be heterogeneous while Tm is constant (28.6±8.9 min with 87.5±0.2 °C), indicating that the same product may initiate at different times (**Figure 1.5F**). This is consistent with our knowledge of the stochastic initiation of LAMP (23,38,39). Further, we observed some variability in the maximum rate despite similar Tm (23.7±6.8 RFU/30 sec, with 87.5±0.2 °C Tm), which indicates the same product may amplify at different velocities. (**Figure 1.5G**). In general, we observed that maximum rate often corresponds to the point when the reaction first began to amplify. Finally, by plotting rate as a function of TTP (**Figure 1.5H**), we observed little fluctuation in rate across a range of different TTPs (23.7±6.8 RFU/30 sec with 28.6±8.9 min), indicating that the differences in TTP are mostly delays in the initiation of amplification rather than differences in the rate of amplification.

The use of real-time data revealed heterogeneity in the timing of amplification initiation and the amplification rate, but homogeneity in Tm, indicating stochasticity in initiation of amplification. In some cases, outlier data points for rate occurred. To determine whether removing these outliers impacted the distribution of enzymatic rates, we performed a non-parametric test (**Supplementary Figure 1.17**) and found no significant differences in enzymatic rates when these outliers were excluded.

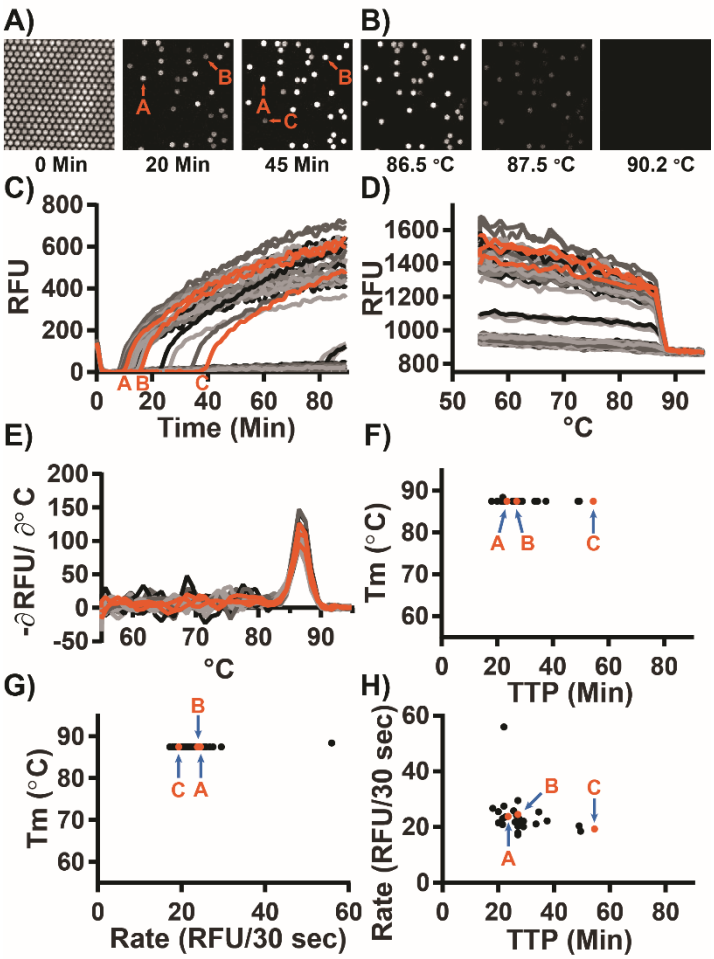

Figure 1.5: Specific amplification in digital single-molecule experiments using *Bst* 2.0. (A) Fluorescence micrographs of individual partitions are traced over time.

For simplicity, we illustrate a subset of 250 of 20,000 possible partitions at three time points (0, 20, and 45 min). Of the 250 partitions in this micrograph, 30 partitions amplified. Partitions A and B are visible at 20 min; partition C becomes visible at 45 min. (B) Fluorescence micrographs of individual partitions are traced across temperatures during an HRM experiment. As the double-stranded DNA in each partition de-hybridizes, the intercalating dye is released and fluorescence decreases. (C) Plotting the fluorescence intensity as function of time generates the standard amplification traces of individual partitions generated during a 90-min LAMP experiment. Orange curves correspond to partitions A–C from panel A. (D) Traces

of fluorescence intensity as a function of temperature for individual partitions during melting experiments. By quantifying real-time intensity of individual partitions as temperature increases, melting traces are obtained. Temperature resolution is 1 °C from 55–90 °C, and 0.5 °C from 90–95 °C. (E) The derivative plot of panel d generates the standard melting curve. The temperature at which the derivative maximum occurs corresponds to the "melting point" of the LAMP products in the individual partition. (F) The time each partition reached a fluorescence intensity of 250 RFU (TTP) as a function of temperature. (G) Maximum rate as a function of Tm for each partition. (H) TTP as a function of maximum rate for each partition.

We next asked whether we could observe in dLAMP the same pattern of high-Tm nonspecific amplification and low-Tm specific amplification that we observed in bulk. We performed dLAMP using three chips containing template, and three chips lacking template (NTC), and observed ~55,000 partitions for each condition. Although 60,000 partitions are possible, not all partitions filled nor can all partitions be tracked for the full duration of an experiment. For the melt curve, fluorescence readings were taken at 1 °C increments from 55-90 °C; and at 0.5 °C increments from 90–95 °C to give higher resolution. Due to slight differences in the timing between the heating element and the image collection, some chips were observed at slightly different temperatures (<0.5 °C).

Our approach enabled us to differentiate specific and nonspecific amplification events using HRM. When using the polymerase *Bst* 2.0 and template (**Figure 1.6A**, blue points), we observed a large band of amplification in the temperature range 88.5–90.3 °C, in agreement with the Tm observed when performing the reaction in bulk (**Figure 1.1**). In contrast, the NTC (**Figure 1.6A**, red points) had very few amplification events in that temperature range (68 out of 51,279 partitions). Hence, we defined events that occurred in the Tm range 88.5–90.3°C as true positives (specific amplification events), and we defined those that occurred outside this range (in both the NTC and in the presence of template) as false positives (nonspecific amplification events). When using the polymerase *Bst* 3.0, we observed a large

band of amplification from 91.25–92.75 °C in the presence of template (**Figure 1.6B**, blue points) that did not correspond with amplification in the NTC (**Figure 1.6B**, red points), so we defined these as specific amplification events. As with bulk measurements, we determined the difference in Tm between specific amplification events between *Bst* 2.0 and *Bst* 3.0 was due to the difference in buffer composition (**Supplementary Figure 1.11, Table 1-1**).

During these experiments, we observed two common patterns. First, the Tm for specific amplification events was 3–5 °C lower in digital compared with bulk measurements. We attribute this difference to temperature calibration; the thermocycler is calibrated to the liquid temperature, whereas the thermoelectric element measures the temperature of the heating element. Second, false positives in the NTC had predominantly high Tm, which we attribute to the nonspecific product we identified in the bulk reactions. We also observed differences in total amplification events between the two polymerases. Assays with *Bst* 3.0 resulted in substantially more nonspecific amplification than those with *Bst* 2.0 and confirmed this was not an issue with buffer selection (**Supplementary Figure 1.11, Table 1-1**). After 90 min, *Bst* 3.0 yielded 15,200 nonspecific events (out of 54,337 observed paritions) in the NTC, whereas *Bst* 2.0 yielded only 74 nonspecific events (out of 51,279) in the NTC. Occasionally, outliers occurred in the NTC and would be misidentified as positives by fluorescence and Tm. For *Bst* 3.0 this occurred in 29 partitions; for *Bst* 2.0, it occurred in only 3 out of ~55,000 partitions.

Next, we tested whether TTP is different for specific and nonspecific amplification. Because LAMP follows a "winner-takes-all" format, frequent and early nonspecific amplification events may dominate bulk amplification. In general, for both *Bst* 2.0 and *Bst* 3.0, specific amplification had earlier TTP than nonspecific amplification, although there was some overlap, mostly >90.5 °C (**Figure 1.6A-B).** We were able to distinguish the clustering of high-Tm nonspecific products separately from specific amplification using a threshold of 88.5–90.3 °C (**Figure 1.6C and Supplementary Figure 1.18A).** We illustrate each partition with only partial opacity so that when false positives in the NTC (red) overlap with false positives in the template-containing sample (blue), the overlap of multiple colors appears

purple (**Figure 1.6D)**. Color intensity indicates the abundance of paritions at a given TTP and temperature. To further illustrate how this approach can be used to differentiate specific and nonspecific amplification, we next selected a region where both specific and nonspecific products were observed**.** For *Bst* 3.0, we were able to distinguish the clustering of high-Tm nonspecific products separately from specific amplification using the threshold of 91.25–92.75 °C **(Figure 1.6E)**, and we observed better separation of specific and nonspecific amplification than with *Bst* 2.0 **(Figure 1.6F and Supplementary Figure 1.18B).** Both enzymes had highly variable TTP, which we have observed previously (23), and attribute to stochastic initiation of LAMP. *Bst* 2.0 had both earlier specific amplification and later nonspecific amplification than *Bst* 3.0. *Bst* 2.0 reactions containing template generally started at 10 min, whereas nonspecific amplification began at ~40 min. In contrast, *Bst* 3.0 reactions containing template began at 11.5 min, and nonspecific amplification began at ~20 min.

Next we asked whether there is a difference between the maximum rates of specific and nonspecific amplification. Previously, we demonstrated that rate could be used to correct for some nonspecific amplification using *E. coli* 23S primers (23), so we wished to test whether we could use maximum rate as a way to differentiate specific and nonspecific amplification. Generally, specific and nonspecific amplification reactions did not have the same maximum rate. For *Bst* 2.0, nonspecific amplification tended to have a slower max rate than specific amplification, although there was some overlap **(Figure 1.6G)**. At high Tm, the clustering of nonspecific amplification in both the presence of template and in the NTC were observed at >90.5 °C and below approximatley 50 RFU/30 sec **(Figure 1.6H)**. For *Bst* 3.0, although there was substantial overlap, we again observed that nonspecific amplification tended to have slower maximum rate than specific amplification **(Figure 1.6I)**. Examining the high-Tm amplification events, nonspecific amplification collects above 92.75 °C and has maximum rate extending out to 75 RFU/30 sec **(Figure 1.6J)**. For both enzymes, overlap between specific and nonspecific amplification was similar, and specific amplification tended to be faster. However, the maximum rate of specific amplification between the two enzymes differed; *Bst* 2.0 had a maxium rate of 150 RFU/30 sec, whereas *Bst* 3.0 did not exceed 100 RFU/30 sec. *Bst* 2.0 performing faster than *Bst* 3.0 is consistent with our previous observations using an *E. Coli* 23S primer set (23). Additionally, the maximum rate of

nonspecific amplification in *Bst* 2.0 tended to be lower than nonspecific amplification in *Bst* 3.0 (50 and 75 RFU/30 sec, respectively). Consequently, the extent of overlap of specific and nonspecific amplificaiton was greater for *Bst* 3.0 than *Bst* 2.0.

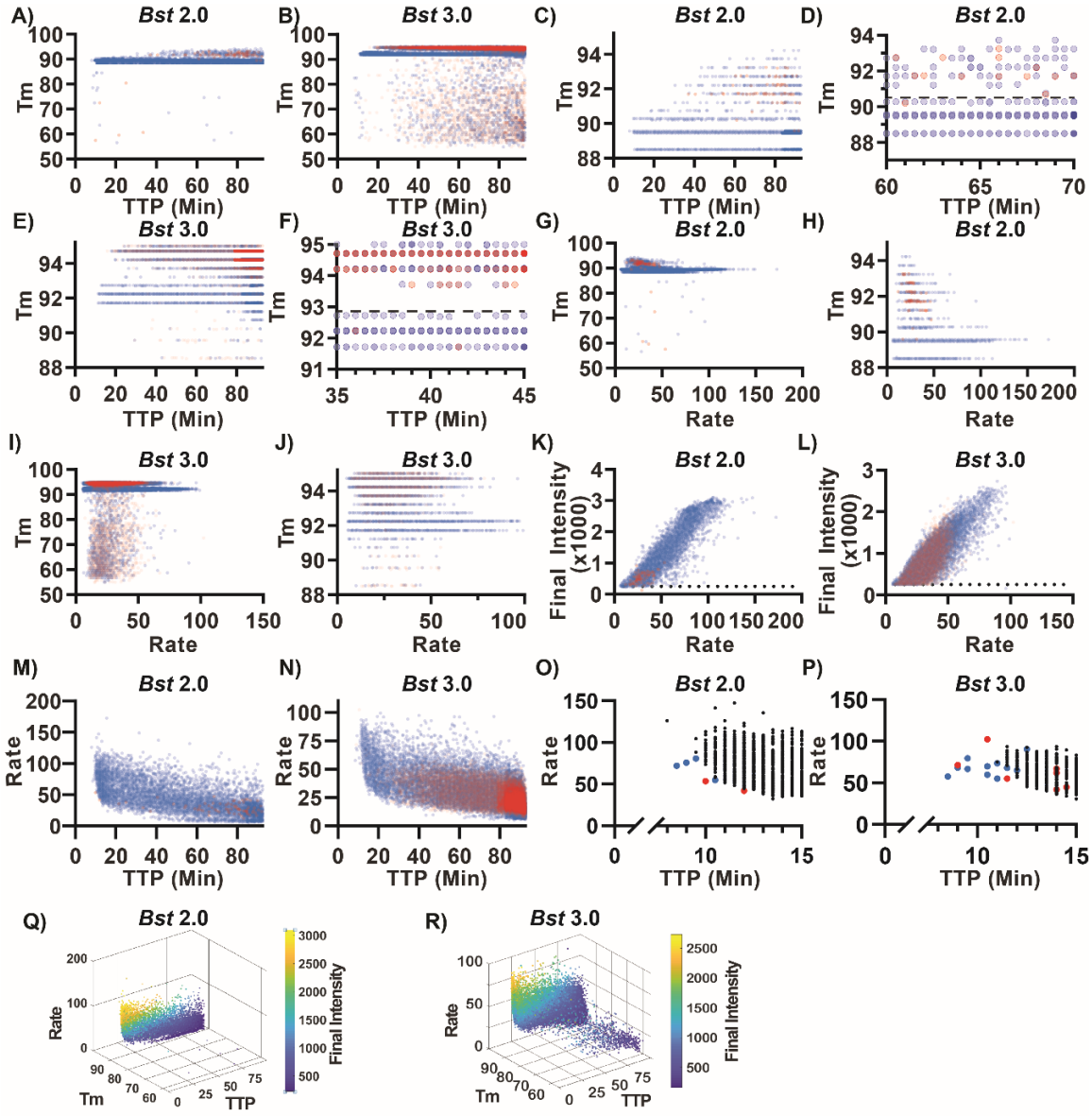

Figure 1.6: Properties of specific and nonspecific amplification using real-time kinetics and Tm.

Blue indicates amplification events in the presence of template, red indicates amplification in the absence of template (NTC). Among these amplification events, true positives were identified using Tm (88.5–90.3 °C for *Bst* 2.0 and 91.25–92.75 °C using *Bst* 3.0). Color intensity indicates the abundance of paritions at a given TTP and temperature (partitions in panels A,C,D,G,H,K,M using *Bst* 2.0 are rendered at 20% opacity in the NTC and in the presence of template; panels B,E,F,I,J,L,N using *Bst* 3.0 are rendered at 5% opacity in the NTC and 20% in the presence of template. (A) Tm of individual amplification events as a function of TTP using *Bst* 2.0. (B) Tm of individual amplification events as a function of TTP using *Bst* 3.0. (C) Individual partitions with Tm between 88 and 95°C as a function of TTP using *Bst* 2.0. (D) Individual partitions with Tm between 88 and 95°C and TTP between 60 and 70 min using *Bst* 2.0. Dashed line at 90.3 °C indicates the upper threshold separating specific and nonspecific amplification. (E) Individual partitions with Tm between 91 and 95°C as a function of TTP using *Bst* 3.0. (F) Individual partitions with Tm between 91 and 95°C and TTP between 35 and 45 min using *Bst* 3.0. Dashed line at 92.75 °C indicates the upper threshold separating specific and nonspecific amplification. (G) Tm of individual amplification events as a function of maximum rate using *Bst* 2.0. (H) Tm of individual amplification events between 88 and 95°C as a function of maximum rate using *Bst* 2.0. (I) Tm of individual amplification events as a function of maximum rate using *Bst* 3.0. (J) Tm of individual amplification events between 88 and 95°C as a function of maximum rate using *Bst* 3.0. (K) The final intensity of individual amplification events as a function of maximum rate using *Bst* 2.0. (L) The final intensity of individual amplification events as a function of maximum rate using *Bst* 3.0. (K-L) Partitions with a final intensity less than 250 RFU (dotted line) were excluded from analyses. (M) The maximum rate of individual amplification events as a function of TTP using *Bst* 2 and (N) using *Bst* 3.0. (O) Plot of maximum rate from false-positive amplifications in NTC (red), false positives amplifications in the presence of template (blue) and true-positive amplifications by Tm (black) as a function of TTP using *Bst* 2.0 and (P) using *Bst* 3.0. (Q) 3D plot comparing maximum

rate, Tm, TTP, and final intensity of individual partitions using *Bst* 2.0 and (R) using *Bst 3*.0.

We observed an unexpected relationship between the final intensity of each partition and the maximum rate of that partition. After 90 min of amplification, a partition should theoretically reach a fluorescence maximum whereby all reagents are consumed, amplification plateaus, and thus the final intensity would be independent of the maximum rate of amplification. However, surprisingly, we observed a general scaling between the maximum rate and the final intensity of the partition. For *Bst* 2.0, all amplification in the NTC has final intensity less than 1017 RFU and maximum rate less than 53.4 RFU/30 sec. In the presence of template, 79.7% of nonspecific amplification and 52.3% of specific amplification had final intensity and maximum rate less than these thresholds. For *Bst* 3.0, 87.7% of amplification in the NTC has final intensity less than 1017 RFU and maximum rate less than 53.4 RFU/30 sec. In the presence of template, 89.0% of nonspecific amplification but only 45.6% of specific amplification fell within these thresholds using Bst 3.0. Thus, false positives were generally dimmer and had slower maximum rates than most true-positive events. When examining the brightest partitions, *Bst* 2.0 (**Figure 1.6K**) and *Bst* 3.0 (**Figure 1.6L**) exhibit a similar maximal final intensity near 3000 RFU. These maxima are also surprising, considering our 12-bit camera is capable of imaging up to 4096 RFU (the detector was not at saturation). We suspect that this maxima corresponds to consumption of one of the reagents; while scaling between maximum rate and final intensity occurs when stochastically initiated reactions have not completely amplified, resulting in partitions dimmer than the maxima and proportional to their rate of amplification.

During these dLAMP experiments, we also observed a relationship between maximum rate and TTP. In bulk reactions, the first and fastest amplification event determines the reaction outcome by consuming all of the reagents. Thus, we hypothesized that reaction conditions that promote fast and early amplification in the NTC would lead to a high false-positive rate in bulk and thus misidentification of amplification. In both *Bst* 2.0 (**Figure 1.6M**) and *Bst* 3.0 (**Figure 1.6N**) we observed a general trend of fast amplification events occurring earlier,

and slow events occurring later. In *Bst* 2.0, we observed greater heterogeneity in TTP and rate than in *Bst* 3.0. Furthermore, nonspecific amplicons in the NTC tended to produce slower and later amplification events. Occasional outliers occurred at both fast and early times.

Next, to explicitly test whether fast and early events correspond to specific amplification, we analyzed the relationship between a partition's TTP, its maximum rate, and Tm. In the first 12 min of amplification, we observed six nonspecific amplification events in *Bst* 2.0 (four in the presence of template; two in the NTC; **Figure 1.6O**), and we observed 13 nonspecific events in *Bst* 3.0 (10 in the presence of template; three in the NTC; **Figure 1.6P**). For both polymerases, we were able to distinguish the rare, fast, and early nonspecific amplicons from true positives. For *Bst* 2.0, these nonspecific amplifications were slower than the fastest true positives, and occurred at similar times. In contrast, for *Bst* 3.0, the earliest amplification events were false positives and tended to have similar rates to the true positives. We hypothesize that in bulk reactions, the fast and early nonspecific amplification events (as seen in *Bst* 3.0 **Figure 1.6P**) lead to nonspecific measurements, whereas nonspecific amplification that coincides with specific amplification, but proceeds at a slower rate (as seen in *Bst* 2.0 **Figure 1.6O**), would still produce specific amplification in bulk. This hypothesis is corroborated by sequencing of bulk LAMP reactions (**Figure 1.2**). Though individual bulk reactions may be assigned a homogeneous label as "true positive" or "false positive" by Tm, sequencing identifies multiple products within each reaction, and the Tm is determined by the dominant product. For example, we observed a "false positive" by Tm (**Figure 1.1C-D)**, despite the presence of template. The sequencing of this product, contained nonspecific product sequences, similar to those observed in the NTC, at high prevalence, as well as the specific target sequences in low abundance (**Figure 1.2 [well C7])**. Similarly, though "true positive" is assigned to other bulk reactions in the presence of template, the nonspecific products are still observed at low abundance (**Figure 1.2 [well F8]**). Further, a greater number of nonspecific partitions in digital using *Bst* 3.0 as compared to *Bst* 2.0, is correlated with a greater number of nonspecific reads despite the presence of template in the sequencing data (Comparing **Figure 1.6A-B** and **Figure 1.2B group A vs C)**. We hypothesize that the combination of real-time parameters (such as rate and TTP), combined with the ability of

digital assays to yield probabilities and to assign reaction identity through HRM, may ultimately help researchers optimize bulk reaction conditions.

A complex interplay exists among TTP, max rate, final intensity, and Tm

To better visualize how TTP, max rate, final intensity, and Tm data are interrelated, we next plotted these data in a four-dimensional (4D) space (**Figure 1.6Q-R, Supplementary Videos S1 and S2 available online**). We observed that among all partitions, regarless of if the product was specific or nonspecific amplificiation, fluorescence was brighter when amplification occurred earlier and faster. This was true for both polymerases. Additionally, we observed two types of nonspecific amplification. The first type of nonspecific was the traditional "primer-dimer" cloud, which is characterized by a low Tm, low final fluorescence intensity, a slow max rate, and a generally late TTP. The second type of nonspecific cloud matches only in its high Tm, and spans a wide range of rates, TTP, and final intensities. The high-Tm nonspecific amplification occurs with greater frequency than the low-Tm nonspecific amplification. The major differences between the polymerases can also be resolved with this visualization. The number of nonspecific amplification events is much fewer for *Bst* 2.0 than for *Bst* 3.0. Further, these nonspecific events in *Bst* 2.0 never achieve same fluorescene intensity or maximum rate as with *Bst* 3.0. We include the 4D representation as part of our MATLAB code, and as videos in the SI.

Classification of true or false positives enables optimal analysis parameter selection

We next asked whether using a combination of digital real-time parameters, in conjunction with Tm, could be used to improve the performance (LOD) of a dLAMP assay. For any given assay, there is a large combination of possible parameters (e.g. amplification rate, TTP, fluorescence intensity) that are used to determine when a digital partition is "on" or "off." Use of these parameters and selection of thresholds will influence assay performance

(analytical specificity and sensitivity). Assay performance is affected by amplification time and the combination of choices of parameters used to process the data impacting LOD, the probability of detecting a molecule (efficiency), and the clinical sensitivity and specificity. Having established that there is a direct relationship between Tm, sequence identity, and structure, we determined that Tm allows us to explicitly differentiate specific and nonspecific amplification in dLAMP, and thus, differentiate true from false positives.

We foresee two separate situations of dLAMP analysis using HRM. The first is where HRM is not incorporated in the final assay, but is used during assay development. Second is the ideal situation for quantitative performance, where HRM is incorporated into the final LAMP assay. We expect the first group of LAMP assays to exist because collecting Tm data adds additional time to an assay and requires more advanced hardware to run. This may be unideal in situations requiring more rapid diagnostics or limited-resource and field settings where the hardware may be impractical. Nonetheless, running HRM is still useful during LAMP assay development to select the optimal combination of parameters for end-point or real-time LAMP without using Tm. Hence, Tm allows one to identify the correct combination of assay parameters, and how to analyze the data for best LOD.

LOD is a key parameter when optimizing clinical assays because pathogen load is low in many infections (e.g. in blood infections or asymptomatic sexually transmitted infections). We thus illustrated the optimization of parameters using improved LOD as the selection criteria. The combination of real-time dLAMP with HRM can uniquely define LOD because of the combination of digital and Tm. Unlike bulk assays, which require a concentration titration curve (and are thus dependent on integrated signal intensity and enzymatic turnover), digital assays only require that an event (target molecule) is or is not observed, and can be counted relative to the partition volume (40,41). The minimum LOD for any digital assay corresponds to one target or amplification event per partition volume. Hence, we can define LOD from a single concentration point by Eq. 1:

Equation 1-1

$$LOD = \frac{C_{True}}{[N_{True} - (N_{False} + 3 \times \sqrt{N_{False}})]/N_{CI}}$$

where C_{True} is the concentration of target molecules loaded by ddPCR counts in copies per microliter, N_{True} is the number of true positive (specific) amplification events observed on a chip, N_{False} is the number of nonspecific amplification events observed on a chip, and N_{CI} is the number of expected molecules for a given confidence interval. In this equation, the N_{True} and N_{False} are chip-specific, and take into account the total volume of the chip, the number of partitions, and the volume of partitions. Furthermore, in Eq. 1, amplification efficiency is implicitly taken into account via the N_{True} parameter (in other words, for a less efficient amplification process, a given C_{True} on a given chip would lead to a lower value of N_{True}). Finally, for simplicity, Eq. 1 makes the assumption that the measurements are performed at sufficiently low concentrations (as is typical for LOD experiments) that only a very small fraction of occupied partitions contain more than one molecule, and therefore, there is a linear relationship between C_{True} and N_{True}.

The concentration loaded, C_{True}, generates N total counts of both true- and false-positive events. We can divide this concentration by the minimal number of counts needed to identify a specific amplification event and define this as the LOD. The minimum number of counts needed to guarantee a specific amplification event is observed is determined by N_{True}, N_{False}, and N_{CI}. N_{True} and N_{False} are determined empirically, whereas N_{CI} is calculated from the desired expected number of molecules that will yield at least one detection event for a given confidence interval (N_{CI}) from the Poisson equation. If we require a 95% CI to observe a true positive across an entire chip, the minimum number of counted events is 3 (i.e. 5% of the time, the Poisson expected loading of 3 target molecules will still measure zero events). For a 98% CI, N_{CI} would be 4 counts. Hence, all true-positive counts in excess of N_{CI} are counts observed above the LOD. Uncertainty in the LOD is given by Supplementary Equations S1-S2.

Counting only true positives does not account for interference from false positives. In order to meet our minimum counts for detection, our equation must remove false counts (N_{False}.) The generally accepted procedure for LOD calculations with a 99.7% CI is to assign N_{True} only when the counts exceed the background plus three standard deviations of the background ($N_{False} + 3 \times \sqrt{N_{False}}$). We approximate the variance in the background using the counting error as three times the square root of the number of false-positive events counted and subtract those counts from the true-positive counts to yield the equation.

Using this calculation of LOD to optimize an assay has three limitations. First, Eq. 1 fails to produce a number with physical meaning when the number of true-positive events (N_{True}) is less than the number of false-positive events plus three times the standard deviation in false amplification ($N_{False} + 3 \times \sqrt{N_{False}}$). In this case, it is not possible to conclusively observe a true positive, and the LOD becomes irrelevant. Second, Eq. 1 gives an absolute LOD. The numerator (concentration of template molecules loaded on the chip, as determined by PCR) is corrected for the probability of observing a molecule amplify (efficiency) by the true-positive counts. N_{False} accounts for the nonspecific amplification, and N_{CI} accounts for the Poisson probability associated with loading a target molecule. Third, this equation is specific to digital assays.

We first sought to demonstrate the selection of optimal parameters for situations where HRM is not incorporated into the final assay. Using this process, one can pick any threshold and use Tm to determine the optimal trade-off between true and false positives. All initial experiments testing the utility of LOD, juxtaposed against receiver operating characteristic (ROC) curves, to identify optimal parameters were done using *Bst* 3.0. We began by determining the optimal thresholds for max rate, fluorescence intensity, and amplification time. We demonstrate optimization of all three parameters, using Tm as the arbiter, to illustrate the utility of our method.

We tested the use of ROC curves (commonly used to indicate clinical sensitivity and specificity) to compare the performance in response to a given parameter. ROC curves provide a visual representation of the ability to distinguish between a true-positive and false-

positive event, as a function of a given threshold, but can be difficult to use for optimal selection of LOD. ROC curves show the fractions of true and false positives, where the true-positive fraction is the number of true positives at a given threshold out of the total number of true positives observed by Tm; and the false-positive fraction is the number of false positives counted at the given threshold, divided by the total number of false positives observed by Tm. A perfect classifying test will yield the largest true-positive fraction and smallest false-positive fraction.

When plotting the ROC curve for maximum rate (**Figure 1.19A**), we observed that rate initially performs very well for eliminating false positives (the false-positive fraction is very small for very high rates). However, as the digital threshold (analogous to ROC "cut-point") for rate decreases, a greater number of both false and true-positive values are counted. Closer examination of this range of thresholds (**Figure 1.19B**) emphasizes the Youden Index at 34.6 true-positive fraction and 4.6 false-positive fraction as a possible choice for optimum threshold, although the assay performance in terms of LOD is unclear. The choice for optimal final-intensity threshold is even less clear with the ROC curve (**Figure 1.19C**), as the ROC curves do not give clear indication of the optimal LOD (the ROC curve is a gentle concave slope). Even relatively high fluorescence thresholds do not give indications of the optimal cut-point (**Figure 1.19D**).

Filtering using LOD revealed a clear optimum. We plot the total number of events for both true and false positives and LOD as a function of maximum rate (**Figure 1.7A**). The LOD curve revealed a clear minima, corresponding to the optimal cut-point using rate. Selecting the threshold of 49.8 RFU/30 seconds generated an LOD of 2.11±0.92 cp/µL. Similarly, plotting LOD against final intensity resulted in a clear minima, despite the histogram appearing as a continuum and the cut-point being thus ambiguous (**Figure 1.7B**). Using final intensity, an LOD of 2.14±0.89 cp/µL can be achieved at 1393 RFU.

The ROC curve for TTP presented a narrow range of thresholds, with ~50% true-positive fraction and 2% false-positive fraction, although the precise optimal threshold was not obvious (**Figure 1.19E**). To refine this threshold, we plotted the LOD and the cumulative

counts as a function of time in both linear (**Figure 1.7C**) and logarithmic scales (**Figure 1.7D**).

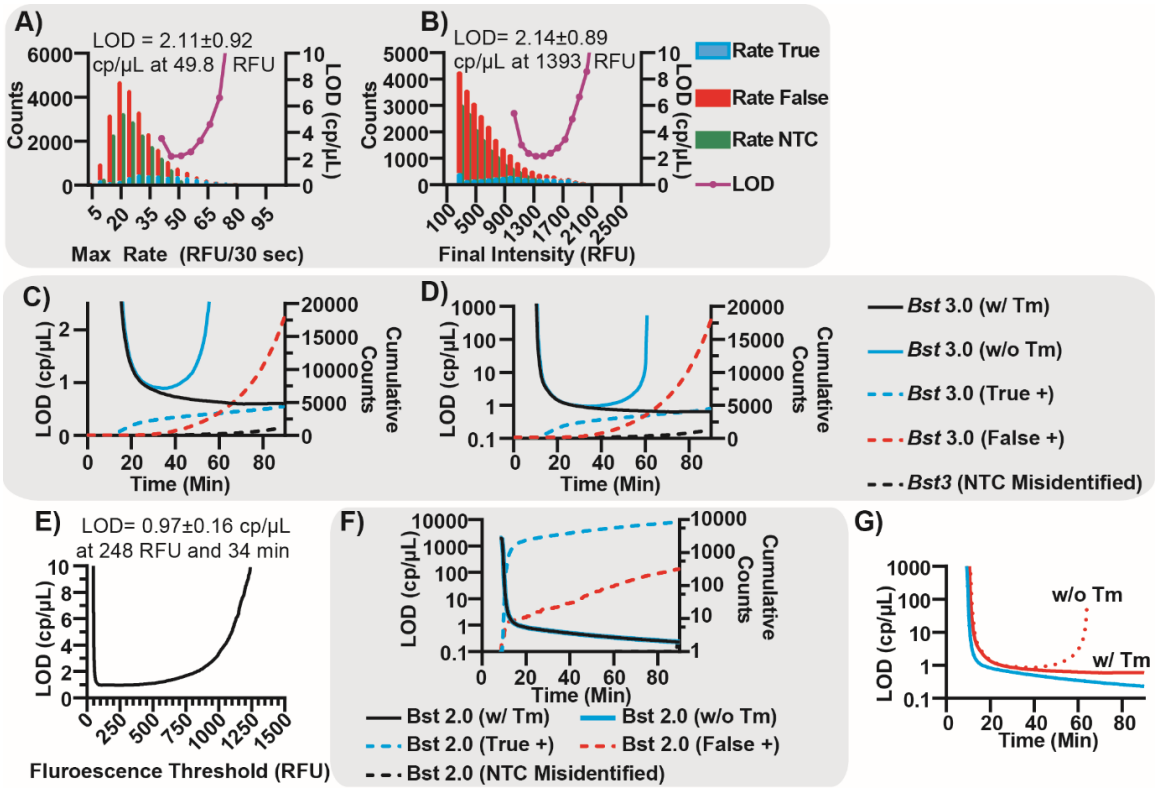

Figure 1.7: Classification of amplification reactions using HRM to determine optimal performance of dLAMP assays.

(A) Histogram of the false positives identified by Tm within the presence of template (red), true positives by Tm (blue), and false positives in the NTC (green), binned by max rate of the partition and a LOD curve plotted as a function of max rate using *Bst* 3.0. B) Histogram of the false positives identified by Tm within the presence of template (red), true positives by Tm (blue), and false positives in the NTC (green), binned by final intensity of the partition and an LOD curve plotted as a function of final intensity using *Bst* 3.0. C) LOD Curves using *Bst* 3.0 as a function of time without using Tm in the final assay (blue) and using Tm in the final device (black). Plots of cumulative counts of true positives (red dashed), false positives (blue

dashed), and incorrectly identified partitions (black dashed). D) Logarithmic plot of LOD curves using *Bst* 3.0 as a function of time without using Tm in the final assay (blue) and using Tm in the final device (black). Plots of cumulative counts of true positives (red dashed), false positives (blue dashed), and incorrectly identified partitions (black dashed). E) LOD plotted as a function of fluorescence intensity, when the assay is measured at the optimal TTP of 34 min. F) Logarithmic plot of LOD curves, using *Bst* 2.0, as a function of time without using Tm in the final assay (blue) and using Tm in the final device (black). The blue and black plots overlay. Plots of cumulative counts of true positives (blue dashed), false positives (red dashed), and incorrectly identified partitions (black dashed). G) Plot of LOD curves as a function of time comparing *Bst* 2.0 (solid blue with Tm, dotted blue without Tm) and *Bst* 3.0 (solid red with Tm, dotted red without Tm). Curves for *Bst* 2.0 overlap.

Assays employing HRM only during the development of the assay can improve the LOD of the final assays by selecting (making an informed choice of the optimum threshold). The LOD decreases (blue curve) as the true positives begin to amplify (blue dashed) and increase, as the false positives amplify (red dashed). The minima for this system occurs at 34 min and 0.93±16 cp/μL, striking a balance between allowing many true positives to amplify, and only a small amount of false positives to occur (53.6% true-positive fraction and 1.5% false-positive fraction) and is clearly defined using the linear scale (**Figure 1.7C**). Plotting of LOD on the logarithmic scale (**Figure 1.7D**) emphasizes improperly selecting a threshold can result in several orders of magnitude loss in assay performance (for example, stopping the assay too early or allowing the assay to run for too long). Although dLAMP is robust to perturbations, selecting the appropriate duration for amplification is important.

In contrast, assays using HRM as part of the final readout can distinguish false positives from the true positives and improve LOD further by excluding nonspecific amplification from the analysis. In some instances, a NTC may incorrectly identify partitions as true positives by Tm (black dashed). We incorporate these events as nonspecific amplification in case HRM is used in the final readout. If nonspecific amplification is eliminated, the assay LOD (**Figure**

1.7C,F, black solid) continues to improve with time, and is only dependent on the stochastic probability that a true positive will initiate and amplify. In this scenario, there is no penalty allowing the assay to amplify for extended periods of time.

In this scenario the LOD equation simplifies to

Equation 1-2

$$LOD = \frac{C_{True}}{N_{True}/N_{CI}} = \sim \frac{N_{CI}}{Fraction\ copies\ detected}$$

Additionally, there is no limitation on the number of parameters that can be used to identify the optimal LOD. Using multiple parameters to filter the data may be useful for individuals not employing HRM in the final assay or in assays only employing end-point measurement (e.g. an assay without real-time measurements will be unable to generate data on rate, but still benefit from selecting optimal assay time and fluorescence threshold). As a demonstration, we filtered first by optimal TTP, then for the optima of a second parameter. In this case, we selected the optimal TTP of 34 min, and scanned for optimal fluorescence threshold. We plotted LOD as a function of fluorescence threshold and determined that the optimal fluorescence threshold at 34 min would be 248 RFU and correspond to an LOD of 0.97±0.16 cp/µL (**Figure 1.7E**).

Do filter parameters exhibit the same LOD minima when using *Bst* 2.0 as they did for *Bst* 3.0? *Bst* 2.0 had much lower nonspecific background than *Bst* 3.0, and could behave similarly or may behave differently.

First, does the ROC curve for TTP display a clear optimum? Similar to the TTP ROC for *Bst* 3.0 (**Figure 1.19E**), the TTP ROC for *Bst* 2.0 has a concave slope making choice of the optimum a matter of computation (**Figure 1.19F**). We can visually estimate the balance of true and false-positive fraction in the range of 50% true and 10% false. Similar curves for max rate and final intensity could be generated but are not shown here.

Second, is there an advantage to using HRM in the final assay with *Bst* 2.0? To answer this question, we plot LOD and the cumulative counts of true and false positives as a function of time for *Bst* 2.0 (**Figure 1.7F**). Similarly to *Bst* 3.0, we observe LOD improve rapidly as true-positive events are counted. However, unlike *Bst* 3.0, the nonspecific amplification events are few, and their presence does not have an impact on LOD. Thus, when using *Bst* 2.0, the curves representing LOD with or without HRM in the final assay overlay and indicate using HRM in the final assay has no additional benefit. Furthermore, the continuously decreasing LOD with time for either case indicates that use of ROC curves to determine an optimum can be misleading. While the ROC implies that an optimum exists, the false-positive incidence is rare enough that a TTP optimum selected by LOD does not exist. Hence, assay developers may select assay time based on requirements other than LOD.

We next assessed whether we could use HRM to compare the performance of the two polymerases, to see which one would give the best LOD and which combination of hardware components would give the optimum assay performance. (**Figure 1.7G**) For both polymerases, we observed a similar, rapid decrease in LOD in the initial moments as true-positive events are detected. However, we also noticed several differences. *Bst* 2.0 has a lower LOD than *Bst* 3.0 at any amplification time. We attribute this difference to the higher incidence of false positives when using *Bst* 3.0 compared with *Bst* 2.0. An additional consequence of the low false-positive incidence using *Bst* 2.0, regardless of the use of HRM in the assay, is the LOD continues to improve with time as additional true positives are counted. In contrast, *Bst* 3.0 benefits greatly from use of HRM in the final assay. If HRM is not included in the assay (**Figure 1.7G**, red dashed), a clear optimum for LOD occurs at 34 min and 0.93±0.16 cp/µL. However, if HRM is employed in the assay, the LOD more closely resembles the LOD curve for *Bst* 2.0 and improves with increased detection of true-positive events.

We made several overarching conclusions regarding improving the LOD of dLAMP using a combination of digital real-time parameters and Tm. First, filter parameters can be used singly or in combination to improve the performance (LOD) of dLAMP. In certain assays, one parameter may perform better than another for this selection. For this primer set, LOD

for *Bst* 3.0 was lower (better) when using TTP (0.93±0.16 cp/µL) than max rate (2.11±0.92 cp/µL) or final intensity (2.14±0.89 cp/µL). Second, incorporation of HRM into the final assay readout will benefit some assays more than others. We observed incorporation of HRM as a part of the final assay improved the perofmance of *Bst* 3.0 greater than the perofmance of *Bst* 2.0, and was vital for long assay times.

Classification demonstrates host genomic DNA alters specific and nonspecific amplification in dLAMP

Assays with high clinical sensitivity and specificity are critically needed. Clinical samples of CT, originating from urine and swabs, pose an intrinsic challenge because they contain variable levels of host DNA and DNA from other flora. The analysis of these clinical samples needs not only to be sensitive (good LOD), but also to be able to function in the presence of nonspecific, potentially amplifiable genomic secondary structures and other possible environmental contaminants, while remaining consistent between samples.

We sought to investigate the impact of host human genomic DNA (hgDNA) on nonspecific background amplification. We hypothesized that nonspecific structures (like hairpins and regulatory elements), may amplify in the presence of LAMP and contribute to nonspecific background amplification. We titrated sheared buffy coat gDNA (i.e. leukocytes) concentrations from zero to $2.5x10^3$ cells per µL, a concentration 2.5x greater than that expected to cause interference (8), and observed the impact on specific and nonspecific amplification of CT (**Figure 1.8**). We measured the concentration of hgDNA in Human Haploid Genome Equivalents (HHGE) or half the total amount of hgDNA in a diploid cell. For each concentration of host DNA and enzyme, we ran at least three chips in the presence of CT template and three in the absence of template across multiple days and sample lots. In total, we observed 1,196,038 different reaction partitions. At the highest concentration of hgDNA, there was 3,030,000 times more hgDNA than bacterial DNA by mass.

We first asked how background DNA impacted TTP qualitatively. We observed for both *Bst* 2.0 and *Bst* 3.0 enzymes, specific and nonspecific amplification were qualitative similar independent of background DNA concentration below 5000 HHGE per µL. As with previous measurements, *Bst* 2.0 rarely produced low-Tm nonspecific events; whereas *Bst* 3.0 produced both high- and low-Tm nonspecific events. Further, there were more nonspecific amplification events for *Bst* 3.0 than *Bst* 2.0 at both high and low Tm.

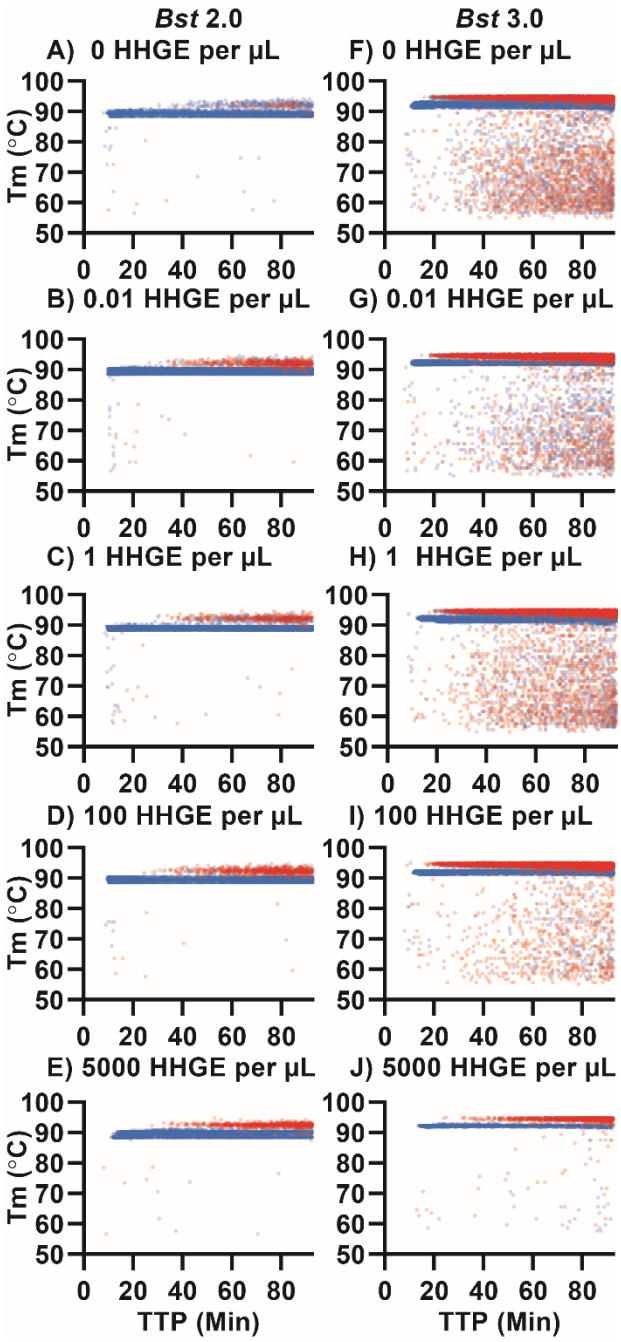

Figure 1.8: Impacts of host (human) genomic DNA in human haploid genome equivalents (HHGE) on specific and nonspecific amplification.

Plots of Tm as a function TTP using *Bst* 2.0 at (A) 0 HHGE per µL; (B) 0.01 HHGE per µL, C) 1 HHGE per µL, D) 100 HHGE per µL, and E) 5000 HHGE per µL; and using *Bst* 3.0 at (F) 0 HHGE per µL, (G) 0.01 HHGE per µL, H) 1 HHGE per µL, I)

100 HHGE per µL J) 5000 HHGE per µL in the presence of template (blue) and NTC (red). N = 3 for all conditions, except *Bst* 3.0 at 0 and 100 HHGE per µL in the presence of template, where N = 6.

We next asked how background hgDNA impacts specific and nonspecific amplification quantitatively. We categorized amplification events as specific and nonspecific based on Tm as previously. First, we asked: Is there a relationship between fraction of template molecules amplified in dLAMP and amplification time? We then determined the total number of template copies loaded into a chip relative to the copies measured by ddPCR. If amplification initiation is stochastic, as observed in **Figure 1.5F** and **Figure 1.6A-B**, does longer assay time increase ”efficiency” and thereby improve LOD when using Tm (as seen in **Figure 1.7C,F**)? We observe that for *Bst* 2.0, a large number of partitions amplify at in the first 11.5 min, followed by a second phase after 20 min where additional partitions amplify with lower frequency (**Figure 1.9A**). The mode TTP for concentrations less than 5000 HHGE per µL was ~11.6±0.2 min (**Table 1-8, Figure 1.20A, Figure 1.21C**). After the mode TTP, the frequency of observing specific amplification in the absence of HHGE decreases from a maximum frequency of 1.2±0.1% copies detected per 30 sec to a lower average frequency of 0.23±0.04 % copies per 30 sec from 20 to 90 min (**Figure 1.9A**). For ***Bst* 3.0** (**Figure 1.20A**), we observe a similar trend temporally, though mode TTP was at least 2 min slower and had greater variability than *Bst* 2.0 (**Table 1-8, Figure 1.20B, Figure 1.21D**). Further, *Bst* 3.0 consistently amplified fewer target molecules than *Bst* 2.0 at all time points. This highlights the stochastic nature of amplification using LAMP and the importance in choice of enzyme on sensitivity. In theory, assays employing Tm could be run until all partitions amplify as either a false or true positive. Allow all partitions to amplify would give the highest possible number of target copies amplified and lowest possible LOD when using Tm in the final assay.

Second, we asked, what is the impact of hgDNA on efficiency as a function of time? For both *Bst* 2.0 and 3.0 (**Figure 1.19A, Figure 1.20A**), when comparing within a given enzyme, we observed that the fraction of copies detected, and the moment the majority of reactions

initiate, were indistinguishable for concentrations less than 5000 HHGE per µL. At 5000 HHGE per µL, a decrease in the fraction of copies detected and a delay in amplification initiation was observed (see also **Figure 1.21C,D**). *Bst* 2.0 had a mode TTP of delay of 4.7 min to 16.3±2.7 min, whereas in *Bst* 3.0, the mode TTP was 17.2±2.1 min at 5000 HHGE per µL (**Table 1-8, Figure 1.21**). Thus, high concentrations of hgDNA may suppress specific amplification.

Third, we asked, what is the impact of hgDNA and time on nonspecific amplification? For *Bst* 2.0, we observed consistent nonspecific amplification products with high and low Tm, regardless of concentration of hgDNA. Single digital partition counts were observed at low-Tm nonspecific amplification in both the presence of template and the NTC and independent of hgDNA concentration (**Figure 1.19B-C**). The fraction of partitions generating a false-positive amplification at low Tm was less than $3.3x10^{-4}$ through 45 min (i.e. 7 or fewer events in 20,000 partitions per chip). Similarly, partition counts of high-Tm nonspecific amplification are <10 per chip until 45 min. After 90 min, high-Tm nonspecific amplification is more prevalent than low-Tm nonspecific amplification, and the reactions finish with fewer than nonspecific 260 counts in 20,000 partitions corresponding to a false-positive fraction of 1.3×10^{-2}. One exception is the nonspecific high-Tm amplification in the absence template and HHGE. This condition appears to have lower nonspecific background than other conditions. We collected each replicate on separate days and were able to observe the experimental variability between the presence and absence fo template, which might be otherwise lost when examining the NTC alone. This experiment emphasizes the advantage of determining nonspecific amplificaiton using Tm from the same experiment as specific amplification is counted. At low background rates, such as when using *Bst* 2.0, inherent variability exists in the false-positive fraction and can impact LOD. Meauring nonspecific amplificaiton from within an experiment eliminates the assumption that the false-positive rate remains identical to the NTC or between experimental runs.

For *Bst* 3.0, nonspecific amplification was variable, but tended to be fewer for higher concentrations of hgDNA. At any given time, high-Tm nonspecific amplification was on average ~30 fold more likely to occur than a low-Tm nonspecific product. At 45 min, low-

Tm nonspecific amplification had false-positive fraction less than $3.1x10^{-3}$ (62 or fewer events per chip), amplification events with high Tm had a false-positive fraction less than $1.9x10^{-2}$ (386 or fewer events per chip). At the completion of the experiment, high-Tm nonspecific amplification events account for as much as 35% of the total partitions per chip; a value exceeding the total observed true-positive events. In these scenarios, utilization of Tm to identify true and false amplification will be critical to successful quantification of target analytes.

For this CT primer set, both *Bst* 2.0 and *Bst* 3.0 similarly demonstrate that the presence of high concentrations of hgDNA may suppress the likelihood of nonspecific amplification occurring. In general, for this primer set and target, we find that *Bst* 2.0 performs significantly better than *Bst* 3.0 as a consequence of having higher probability of detecting a target molecule and low likelihood of generating a nonspecific amplification event.

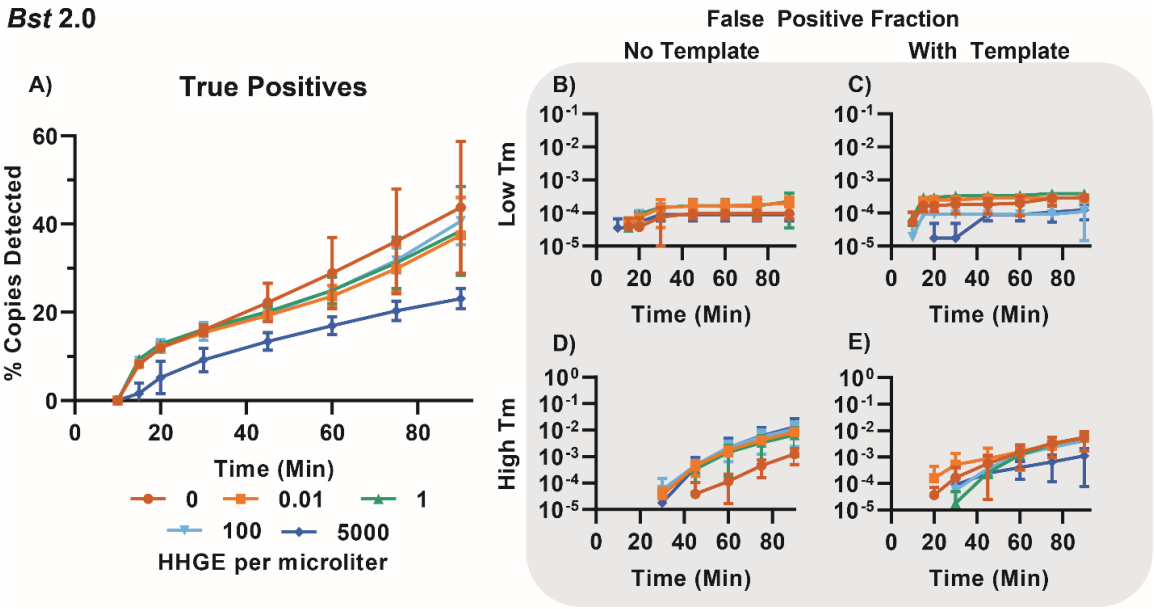

Figure 1.9: Quantification of the impact of hgDNA on specific and nonspecific amplification using *Bst* 2.0 a as a function of time.

(A) Plot of the % copies detected (specific amplification) as a function of time. (B-C) The fraction of partitions with nonspecific amplification with Tm less than the specific amplification in the NTC (B) and in the presence of template (C) as a function of time. (D-E) The fraction of partitions with nonspecific amplification with Tm greater than the specific amplification in the NTC (D) and in the presence of template (E) as a function of time. Panel (A) is available in tabular form as Supplementary **Table 1-9**.

Fourth, we asked, is maximum rate impacted by the concentration of hgDNA? We hypothesize that background hgDNA may compete for the binding site of the polymerase with the target DNA or generate competing amplification events and thus, decrease the maximum observed velocity in a given partition. This phenomena would be challenging to untangle in bulk. We find that maximum rates are similar for a given enzyme, until 5000 HHGE per µL for *Bst* 2.0 (**Figure 1.21A**), and above 100 HHGE per µL for *Bst* 3.0 (**Figure 1.21B**). Thus demonstrating that high concentrations of HHGE may slow the rate of amplification. Furthermore, in general, and echoing the conclusions of **Figure 1.6G,I**, we observe that *Bst* 2.0 has faster maximum rate than *Bst* 3.0, regardless of the hgDNA concentration.

Fifth, we asked, how is LOD impacted by the concentration of hgDNA? For *Bst* 2.0 (**Figure 1.21E**), the LOD at a given time was similar for concentrations less than 5000 HHGE per µL. Meanwhile, the LOD in the presence of 5000 HHGE per µL was slightly worse as evidenced by the detection of fewer target molecules (e.g. 0.7 vs 0.5 cp/µL at 45 min). As previously, incorporation of HRM into the final assay does not impact the LOD when using *Bst* 2.0. When using *Bst* 3.0 (**Figure 1.21F**) and HRM to remove nonspecific amplification, LOD tracks with the number of true-positive events. Thus, LOD becomes worse when efficiency is lower (i.e., at 5000 HHGE per µL). Similarly, when HRM is not incorporated in the assay, higher concentrations of HHGE tend to result in a worse LOD. However, at long amplification times, high concentrations of HHGE suppress nonspecific amplification

more than specific amplification, resulting in LOD enhancement relative to low concentrations of HHGE.

Cumulatively, these data show high background DNA may reduce the probability of detecting a specific molecule (analytical sensitivity), suppress the false-positive fraction (analytical specificity), reduce the velocity of amplification, and delay the start of amplification at clinically relevant concentrations of hgDNA. Thus, we conclude background hgDNA impacts dLAMP for this primer set. Generally, investigators should examine their own primer sets in the presence of high concentrations of hgDNA and take caution when examining clinical samples with high leukocyte concentrations (as reported by urinanalysis). For example, CT infection is not inherently associated with high concentrations of leukocytes, and many infections are asymptomatic. Ultimately, these experiments underscore the value of quantifying nonspecific amplificaiton variability, using HRM, from within the same experiment as a target is quantified. Because nonspecific amplificaiton is measured within a given sample, one no longer needs to assume it remains identical to the NTC or between experimental runs.

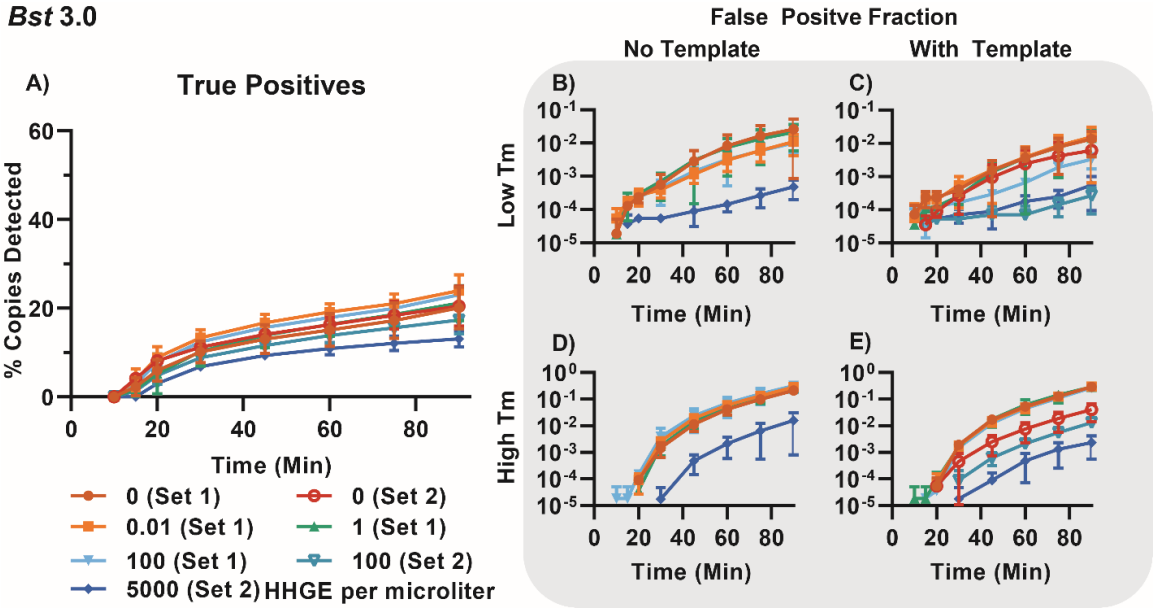

Figure 1.10: Quantification of the impact of hgDNA on specific and nonspecific amplification using *Bst* 3.0 as a function of time.

(A) The percentage copies detected (specific amplification) as a function of time. (B-C) The fraction of partitions with nonspecific amplification with Tm less than the specific amplification in the NTC (B) and in the presence of template (C) as a function of time. (D-E) The fraction of partitions with nonspecific amplification with Tm greater than the specific amplification in the NTC (D) and in the presence of template (E) as a function of time. Panel (A) is available in tabular form as Supplementary **Table 1-10**.

Conclusions

We predict that the combination of HRM and real-time dLAMP will be invaluable for answering many questions across a wide variety of applications, and thus our approach was designed to be accessible to most standard labs. We employed commercial chips for digitization, a commercial thermoelectric unit for heating and cooling, a commercial microscope for optical analyses, and we made our data-processing script freely available. Our intention was to design an accessible system with readily available components to enable

others to access the advantages of digital microfluidics to study and optimize primer sets, enzymes, and reaction conditions of interest to them. We predict these capabilities will be particularly valuable for people working with variable sample matrixes, high background DNA, poorly performing primer sets, or poorly performing enzymes.

We derived four major lessons from this study. First, LAMP can produce nonspecific amplicons with high Tm. The formation of these nonspecific amplicons occurs from the interaction of multiple primers and the use of a polymerase with template switching ability, terminal transferase activity, and lacking 3′–5′ exonuclease activity. Interaction of primers may lead not only lead to rising background fluorescence (37), but to spontaneous exponential amplification as well. Primer design and enzyme selection therefore should be judicious to avoid formation of hairpins within primers, as well as microhomology at the 3' with any other primer, in order to prevent nonspecific amplification.

Second, HRM in LAMP is a useful method for differentiating specific and nonspecific amplification events. Digital experiments measure the fate and rate of each template, in contrast, bulk experiments are biased towards early amplification events. The combination of dLAMP and HRM allows observation of many amplification events and assignment of the nature of that amplification as true or false. Further, dLAMP with HRM quantifies nonspecific amplification experimentally in the presence of specific amplification, eliminating the assumption that incidence of false positives in the presence of template remains identical to the NTC or between experimental runs.

Third, by differentiating specific and nonspecific amplification, HRM is helpful in determining the combination processing and assay parameters that will lead to the best LOD in a digital assay. When HRM is incorporated into a dLAMP assay, true and false-positive amplification events can easily be separated. LOD is improved by elimination of nonspecific background and thus becomes dependent on the number of molecules that amplify (i.e. amplification efficiency or fraction of copies detected), without dependence on the incidence of false positives. In contrast, if HRM were employed in a bulk reaction, the LOD would still be limited by the competition between specific and nonspecific amplification (which

amplifies first) and would require a high number of trials to achieve sufficient statistical power. Importantly, even when HRM will not be used in the final assay, it can still be incorporated during the assay-development stage to improve the assay's LOD by determining the optimal choice of parameters based on rate, TTP, final intensity, or any combination of these parameters. Furthermore, our mathematical description of LOD is generalizable to other amplification methods that are measured in digital and can separate specific and nonspecific amplification.

Fourth, high levels of nonspecific host gDNA suppress analytical sensitivity and specificity, reduce amplification velocity, and delay the start of amplification. However, low-to-moderate levels of nonspecific host gDNA do not impact the analytical specificity or sensitivity of dLAMP. We ran our assays through clinically relevant concentrations of background DNA and did not observe interference until the upper range of concentrations expected to cause interference to demonstrate the clinical utility of real-time dLAMP with HRM.

Real-time dLAMP with HRM will enable the mechanistic optimization of primers and myriad assay conditions (such as buffer, Mg^{2+}, and reaction temperature). Because real-time dLAMP with HRM reveals the incidence of nonspecific amplification products with high and low Tm as a function of time, dLAMP with HRM can be used to investigate approaches that will eliminate different nonspecific products. For example, fast or early nonspecific events in digital may indicate primers or conditions that will be especially vulnerable to failure in a bulk reaction. Thus, real-time dLAMP with HRM could be used to design primers that will suppress nonspecific amplification in bulk, by generating only nonspecific amplicons that occur at slow rates and late TTP.

Future efforts should investigate the combination of real-time dLAMP (and other digital isothermal amplification technologies) and HRM as a way to increase multiplexing of dLAMP when using a single reporter. In PCR, HRM has been used to differentiate among multiple amplification products by measuring differences in Tm (42-46), with applications that include among others multiplexed pathogen identification and antibiotic susceptibility

testing. Finally, studies with clinical samples should be performed using the dLAMP with HRM method to understand the carryover effects from relevant matrices.

Data Availability

The complete sequencing data generated during this study are available in the National Center for Biotechnology Information Sequence Read Archive repository with the BioProject ID: PRJNA574638.

The MATLAB script described here has been deposited in the open-access online repository GitHub and may be accessed using the following direct link:

https://github.com/IsmagilovLab/Digital_NAAT_2Ch_MeltCurve_Analyzer

References

1. Kong, J.E., Wei, Q., Tseng, D., Zhang, J., Pan, E., Lewinski, M., Garner, O.B., Ozcan, A. and Di Carlo, D. (2017) Highly Stable and Sensitive Nucleic Acid Amplification and Cell-Phone-Based Readout. *ACS Nano*, **11**, 2934-2943.

2. Phillips, E.A., Moehling, T.J., Bhadra, S., Ellington, A.D. and Linnes, J.C. (2018) Strand Displacement Probes Combined with Isothermal Nucleic Acid Amplification for Instrument-Free Detection from Complex Samples. *Anal. Chem.*, **90**, 6580-6586.

3. Notomi, T., Okayama, H., Masubuchi, H., Yonekawa, T., Watanabe, K., Amino, N. and Hase, T. (2000) Loop-mediated isothermal amplification of DNA. *Nucleic Acids Res.*, **28**, e63-e63.

4. Somboonna, N., Choopara, I., Arunrut, N., Sukhonpan, K., Sayasathid, J., Dean, D. and Kiatpathomchai, W. (2018) Rapid and sensitive detection of Chlamydia

trachomatis sexually transmitted infections in resource-constrained settings in Thailand at the point-of-care. *PLoS Negl. Trop. Dis.*, **12**, e0006900-e0006900.

5. Ljubin-Sternak, S. and Meštrović, T. (2014) Chlamydia trachomatis and Genital Mycoplasmas: Pathogens with an Impact on Human Reproductive Health. *Journal of pathogens*, **2014**, 183167-183167.

6. Su, W.H., Tsou, T.S., Chen, C.S., Ho, T.Y., Lee, W.L., Yu, Y.Y., Chen, T.J., Tan, C.H. and Wang, P.H. (2011) Diagnosis of Chlamydia infection in women. *Taiwan. J. Obstet. Gynecol.*, **50**, 261-267.

7. McEnroe, R.J., Burritt, M.F., Powers, D.M., Rheinheimer, D.W. and Wallace, B.H. (2018), pp. 112.

8. CLSI. (2005) *Interference Testing in Clinical Chemistry, EP07-A2*. Clinical and Laboratory Standards Institute, Wayne, PA.

9. Schneider, L., Blakely, H. and Tripathi, A. (2019) Mathematical model to reduce loop mediated isothermal amplification (LAMP) false-positive diagnosis. *Electrophoresis*, **40**, 2706-2717.

10. Chou, P.H., Lin, Y.C., Teng, P.H., Chen, C.L. and Lee, P.Y. (2011) Real-time target-specific detection of loop-mediated isothermal amplification for white spot syndrome virus using fluorescence energy transfer-based probes. *J. Virol. Methods*, **173**, 67-74.

11. Gadkar, V.J., Goldfarb, D.M., Gantt, S. and Tilley, P.A.G. (2018) Real-time Detection and Monitoring of Loop Mediated Amplification (LAMP) Reaction Using Self-quenching and De-quenching Fluorogenic Probes. *Sci. Rep.*, **8**, 5548.

12. Ball, C.S., Light, Y.K., Koh, C.-Y., Wheeler, S.S., Coffey, L.L. and Meagher, R.J. (2016) Quenching of Unincorporated Amplification Signal Reporters in Reverse-Transcription Loop-Mediated Isothermal Amplification Enabling Bright, Single-

Step, Closed-Tube, and Multiplexed Detection of RNA Viruses. *Anal. Chem.*, **88**, 3562-3568.

13. Tanner, N.A., Zhang, Y. and Evans, T.C. (2012) Simultaneous multiple target detection in real-time loop-mediated isothermal amplification. *BioTechniques*, **53**, 81-89.

14. Kouguchi, Y., Fujiwara, T., Teramoto, M. and Kuramoto, M. (2010) Homogenous, real-time duplex loop-mediated isothermal amplification using a single fluorophore-labeled primer and an intercalator dye: Its application to the simultaneous detection of Shiga toxin genes 1 and 2 in Shiga toxigenic Escherichia coli isolates. *Mol. Cell. Probes*, **24**, 190-195.

15. Kubota, R., M. Alvarez, A., Su, W.W. and M. Jenkins, D. (2011) FRET-Based Assimilating Probe for Sequence-Specific Real-Time Monitoring of Loop-Mediated Isothermal Amplification (LAMP). *Biological Engineering Transactions*, **4**, 81-100.

16. Jiang, Y.S., Bhadra, S., Li, B., Wu, Y.R., Milligan, J.N. and Ellington, A.D. (2015) Robust strand exchange reactions for the sequence-specific, real-time detection of nucleic acid amplicons. *Anal. Chem.*, **87**, 3314-3320.

17. Liu, W., Huang, S., Liu, N., Dong, D., Yang, Z., Tang, Y., Ma, W., He, X., Ao, D., Xu, Y. *et al.* (2017) Establishment of an accurate and fast detection method using molecular beacons in loop-mediated isothermal amplification assay. *Sci. Rep.*, **7**, 40125.

18. Bhadra, S., Jiang, Y.S., Kumar, M.R., Johnson, R.F., Hensley, L.E. and Ellington, A.D. (2015) Real-Time Sequence-Validated Loop-Mediated Isothermal Amplification Assays for Detection of Middle East Respiratory Syndrome Coronavirus (MERS-CoV). *PLoS One*, **10**, e0123126.

19. Li, B., Chen, X. and Ellington, A.D. (2012) Adapting enzyme-free DNA circuits to the detection of loop-mediated isothermal amplification reactions. *Anal. Chem.*, **84**, 8371-8377.

20. Wan, L., Chen, T., Gao, J., Dong, C., Wong, A.H.-H., Jia, Y., Mak, P.-I., Deng, C.-X. and Martins, R.P. (2017) A digital microfluidic system for loop-mediated isothermal amplification and sequence specific pathogen detection. *Sci. Rep.*, **7**, 14586-14586.

21. Selck, D.A., Karymov, M.A., Sun, B. and Ismagilov, R.F. (2013) Increased robustness of single-molecule counting with microfluidics, digital isothermal amplification, and a mobile phone versus real-time kinetic measurements. *Anal. Chem.*, **85**, 11129-11136.

22. Sun, B., Shen, F., McCalla, S.E., Kreutz, J.E., Karymov, M.A. and Ismagilov, R.F. (2013) Mechanistic evaluation of the pros and cons of digital RT-LAMP for HIV-1 viral load quantification on a microfluidic device and improved efficiency via a two-step digital protocol. *Anal. Chem.*, **85**, 1540-1546.

23. Rolando, J.C., Jue, E., Schoepp, N.G. and Ismagilov, R.F. (2019) Real-Time, Digital LAMP with Commercial Microfluidic Chips Reveals the Interplay of Efficiency, Speed, and Background Amplification as a Function of Reaction Temperature and Time. *Anal. Chem.*, **91**, 1034-1042.

24. Selck, D.A. and Ismagilov, R.F. (2016) Instrument for Real-Time Digital Nucleic Acid Amplification on Custom Microfluidic Devices. *PLoS One*, **11**, e0163060.

25. Njiru, Z.K., Mikosza, A.S.J., Armstrong, T., Enyaru, J.C., Ndung'u, J.M. and Thompson, A.R.C. (2008) Loop-mediated isothermal amplification (LAMP) method for rapid detection of Trypanosoma brucei rhodesiense. *PLoS Negl. Trop. Dis.*, **2**, e147-e147.

26. Tone, K., Fujisaki, R., Yamazaki, T. and Makimura, K. (2017) Enhancing melting curve analysis for the discrimination of loop-mediated isothermal amplification products from four pathogenic molds: Use of inorganic pyrophosphatase and its effect in reducing the variance in melting temperature values. *J. Microbiol. Methods*, **132**, 41-45.

27. Uemura, N., Makimura, K., Onozaki, M., Otsuka, Y., Shibuya, Y., Yazaki, H., Kikuchi, Y., Abe, S. and Kudoh, S. (2008) Development of a loop-mediated isothermal amplification method for diagnosing Pneumocystis pneumonia. *J. Med. Microbiol.*, **57**, 50-57.

28. Liu, N., Zou, D., Dong, D., Yang, Z., Ao, D., Liu, W. and Huang, L. (2017) Development of a multiplex loop-mediated isothermal amplification method for the simultaneous detection of Salmonella spp. and Vibrio parahaemolyticus. *Sci. Rep.*, **7**, 45601.

29. Ayukawa, Y., Hanyuda, S., Fujita, N., Komatsu, K. and Arie, T. (2017) Novel loop-mediated isothermal amplification (LAMP) assay with a universal QProbe can detect SNPs determining races in plant pathogenic fungi. *Sci. Rep.*, **7**, 4253.

30. Hafner, G.J., Yang, I.C., Wolter, L.C., Stafford, M.R. and Giffard, P.M. (2001) Isothermal amplification and multimerization of DNA by Bst DNA polymerase. *BioTechniques*, **30**, 852-856, 858, 860 passim.

31. Wang, G., Ding, X., Hu, J., Wu, W., Sun, J. and Mu, Y. (2017) Unusual isothermal multimerization and amplification by the strand-displacing DNA polymerases with reverse transcription activities. *Sci. Rep.*, **7**, 13928.

32. Zyrina, N.V., Zheleznaya, L.A., Dvoretsky, E.V., Vasiliev, V.D., Chernov, A. and Matvienko, N.I. (2007) N.BspD6I DNA nickase strongly stimulates template-independent synthesis of non-palindromic repetitive DNA by Bst DNA polymerase. *Biol. Chem.*, **388**, 367-372.

33. Garcia, P.B., Robledo, N.L. and Islas, A.L. (2004) Analysis of non-template-directed nucleotide addition and template switching by DNA polymerase. *Biochemistry*, **43**, 16515-16524.

34. Ramadan, K., Shevelev, I.V., Maga, G. and Hübscher, U. (2004) De Novo DNA Synthesis by Human DNA Polymerase λ, DNA Polymerase μ and Terminal Deoxyribonucleotidyl Transferase. *J. Mol. Biol.*, **339**, 395-404.

35. Zyrina, N.V., Antipova, V.N. and Zheleznaya, L.A. (2014) Ab initio synthesis by DNA polymerases. *FEMS Microbiol. Lett.*, **351**, 1-6.

36. Voisey, J., Hafner, G.J., Morris, C.P., van Daal, A. and Giffard, P.M. (2001) Interrogation of Multimeric DNA Amplification Products by Competitive Primer Extension Using Bst DNA Polymerase (Large Fragment). *BioTechniques*, **31**, 1122-1129.

37. Meagher, R.J., Priye, A., Light, Y.K., Huang, C. and Wang, E. (2018) Impact of primer dimers and self-amplifying hairpins on reverse transcription loop-mediated isothermal amplification detection of viral RNA. *Analyst*, **143**, 1924-1933.

38. Khorosheva, E.M., Karymov, M.A., Selck, D.A. and Ismagilov, R.F. (2016) Lack of correlation between reaction speed and analytical sensitivity in isothermal amplification reveals the value of digital methods for optimization: validation using digital real-time RT-LAMP. *Nucleic Acids Res.*, **44**, e10.

39. Tanner, N.A. and Evans, T.C. (2014) Loop-Mediated Isothermal Amplification for Detection of Nucleic Acids. *Curr. Protoc. Mol. Biol.*, **105**, 15.14.11-15.14.14.

40. Rissin, D.M., Kan, C.W., Campbell, T.G., Howes, S.C., Fournier, D.R., Song, L., Piech, T., Patel, P.P., Chang, L., Rivnak, A.J. *et al.* (2010) Single-molecule enzyme-linked immunosorbent assay detects serum proteins at subfemtomolar concentrations. *Nat. Biotechnol.*, **28**, 595-599.

41. Rissin, D.M. and Walt, D.R. (2006) Digital Concentration Readout of Single Enzyme Molecules Using Femtoliter Arrays and Poisson Statistics. *Nano Lett.*, **6**, 520-523.

42. Athamanolap, P., Hsieh, K., Chen, L., Yang, S. and Wang, T.-H. (2017) Integrated Bacterial Identification and Antimicrobial Susceptibility Testing Using PCR and High-Resolution Melt. *Anal. Chem.*, **89**, 11529-11536.

43. Velez, D.O., Mack, H., Jupe, J., Hawker, S., Kulkarni, N., Hedayatnia, B., Zhang, Y., Lawrence, S. and Fraley, S.I. (2017) Massively parallel digital high resolution melt for rapid and absolutely quantitative sequence profiling. *Sci. Rep.*, **7**, 42326.

44. O'Keefe, C.M., Pisanic, T.R., Zec, H., Overman, M.J., Herman, J.G. and Wang, T.-H. (2018) Facile profiling of molecular heterogeneity by microfluidic digital melt. *Science Advances*, **4**, eaat6459.

45. Athamanolap, P., Hsieh, K., O'Keefe, C.M., Zhang, Y., Yang, S. and Wang, T.H. (2019) Nanoarray Digital Polymerase Chain Reaction with High-Resolution Melt for Enabling Broad Bacteria Identification and Pheno-Molecular Antimicrobial Susceptibility Test. *Anal. Chem.*

46. O'Keefe, C.M., Kaushik, A.M. and Wang, T.H. (2019) Highly Efficient Real-Time Droplet Analysis Platform for High-Throughput Interrogation of DNA Sequences by Melt. *Anal. Chem.*, **91**, 11275-11282.

Supporting Information

Primer Sequences

Primers had the following sequences:

- BIP: AAG CAC GCG GAC GAT TGG AAA AAA GCG GAT TTG CCT AAC CG

- BOP: CGA ACA TTC CCC TTG ATC GC
- FIP: GCT GCT CCA TCG TCT ACG CAG TTT TGC TCG TCT TCC CTG GGT T
- FIP_{Short}: GCT GCT CCA TCG TCT ACG CAG TTT TGC TCG TCT TCC CTG GG
- FOP: CCA AGG TTT CCA GGG TCA A
- LoopB: CCG TAG AGC GAT GAG AAC G
- LoopF: GCC TCA ACT TAG GGG CCG

Fabrication of thermoelectric unit mount

Starting from 1/4" thick aluminum stock; a block was squared and milled to 58x61 mm and slightly less than ¼" thick. Both the side in contact with the microfluidic chips and with the thermoelectric unit were finished with a single pass of a ½" fly bit to generate a mirror finish. Four holes for screws holes were counter bored to ensure the heads remained below the surface of the block and mounted to a 1.1 °C/W Half Brick DC Converter Heat Sink (AAVID, via Newark Electronics, 241214B92200G) using four #6-32, 5/8" long screws. A 7/16" hole was clearance drilled into the side of the aluminum to ¾" depth and a thermistor (TE Tech, MP-3002) was inserted and mounted using Thermal Compound (Arctic Alumina Silver Ceramic Polysynthetic). The thermoelectic unit was mounted between the aluminum block and heat sink using Thermal Compound and the screws finger tightened. Desired torque was calculated to be 0.89-7.175 ft*lbs per screw (total pressure 70-170 psi).

Once mounted, a QuantStudio chip was place on top of the block (to mimic total load on the instrument) and the PID tuned following instructions from the TC-720 Controller manual. With I&D set at zero; P was found to oscillate at 1.35 at 70 °C (the expected dLAMP temperature). The oscillation period was 6 seconds. Thus, the Proportional BW was set at 1.7*1.35 = **2.3**. The Integral gain was calculated as I = 1.2/T in min = 1.2/0.1 = **12**. The

derivative gain was calculated as 0.075xT=0.075*0.1= 0.0075 min. With these settings, the observed temperature overshoot from room temperature to 70 °C at maximum output was 0.05 °C, whereas at 95 °C the observed overshoot was 1 °C.

The ability of the embedded thermocouple to accurately assess temperature of the aluminum block was verified with an independent K-type mini-thermcouple read through a General IRT659K [IR] Thermometer.

MATLAB script

The MATLAB script works as follows: First, the TIF stack containing 2-channel images of the LAMP amplification and melt curve along with a .txt file containing temperature over time data are loaded into memory. We used the first image of the ROX channel to define all of the partitions. A custom iterative thresholding algorithm was applied to detect partitions despite lighting non-uniformities, imaging artifacts, or possible debris. The size of a well was pre-defined using the areaBound parameter. For our study, we defined partitions as having areas between 20 to 45 pixels. The algorithm scans through increasing threshold sensitivities, applies the partition size filter, and combines the results into a final mask. This is repeated for each image in the stack.

In order to track the partition intensities over time, it is important to track the same partition. This is challenging because partition move due to thermal expansion during the LAMP heating and melt curve, partitions touching the edge of the image may appear or disappear from the field of view, and bubbles during the melt curve can distort image. To account for this, we applied the built-in MATLAB labeling function to the first image of the stack to assign a unique number to each partition. We assume that a partition will not translate a distance greater than its radius from frame to frame. Using this, we find the centroid of each labeled partition in the first frame and overlay this with the second frame. If a labeled centroid overlaps a partition, the entire partition is assigned the label. If not, the partition was not found and was discarded from the analysis. This method is repeated for the centroids of the

second frame onto partition of the third frame and so on. On average, more than 18,000 of the 20,000 partitions were attained for analysis, which is plenty for statistical confidence.

To analyze partitions, the intensity of each partition is averaged for each frame and plotting against time for the LAMP curve. The data is smoothed using a Gaussian blur, using the gaussWinSize parameter, with window size of 5 frames. The background baseline is subtracted from the LAMP curve. It is calculated by averaging the intensities from the six frames after the temperature of the experiment reached the optimal LAMP temperature. Time to positive (TTP) was calculated as the frame at which the intensity crossed a threshold of 250 RFU, defined using the "threshold" parameter. The derivative of the LAMP curve was calculated and the maximum slope was determined for each curve.

Partitions of interest for melt curve analysis were identified by exceeding a minimum intensity or slope (rate) threshold. Once selected, the average partition intensities during HRM were determined and smoothed similarly as for the LAMP curves. Using the temperature and time data from the .txt file, the melt intensities were replotted with temperature as the x-axis. The negative derivative of the melt curve was used to calculate the peak melt temperature for each partition. We have reported other processing parameters previously (22).

The following processing parameters were used:

- mask_thresh = .08:.002:.16;
- areaBound = [20 45] Pixels;
- threshold = 250 RFU;
- gaussWinSize = 5 Frames;
- maxSlope = 200 RFU/Frame;
- maxSlopeThreshold = 30 RFU/Frame;

- time between Frames (“time_spacing”) = 30 sec;
- LAMP Start (“LAMP_start”) = Frame 1;
- LAMP End (“LAMP_end”) = Frame 185;
- melt Curve Start (“MC_start”) = Frame 194;
- melt Curve End (“MC_end”) = Frame 241;

Propagation of LOD uncertainty

The digital loading of molecules onto a chip is a Poisson process. However, because the number of counting events is large, we can assume the counting events are approximately normally distributed, parameterized by a mean and standard deviation, σ. When measured quantities are normally distributed, then the error in any derived quantities can be found with the following expression (46):

Equation 1-3

$$\sigma_x^2 = \left(\frac{\delta x}{\delta a}\right)^2 \sigma_a^2 + \left(\frac{\delta x}{\delta b}\right)^2 \sigma_b^2 + \ldots \left(\frac{\delta x}{\delta n}\right)^2 \sigma_n^2$$

In our specific scenario, the variance of the derived quantity LOD (Equation 1) can be expressed as:

Equation 1-4

$$\sigma_{LOD}^2 = \left(\frac{1}{[N_{True} - (N_{False} + 3\sqrt{N_{False}})]/N_{CI}}\right)^2 (\sigma_{C_{True}})^2 + \left(-\frac{C_{True}}{([N_{True} - (N_{False} + 3\sqrt{N_{False}})]/N_{CI})^2}\right)^2 (\sigma_{N_{True}})^2 + \left((-\frac{C_{True}}{([N_{True} - (N_{False} + 3\sqrt{N_{False}})]/N_{CI})^2})(-\frac{1}{N_{CI}} - \frac{3}{2N_{CI}\sqrt{N_{False}}})\right)^2 (\sigma_{N_{False}})^2$$

Impact of buffer conditions on specific and nonspecific amplification and Tm

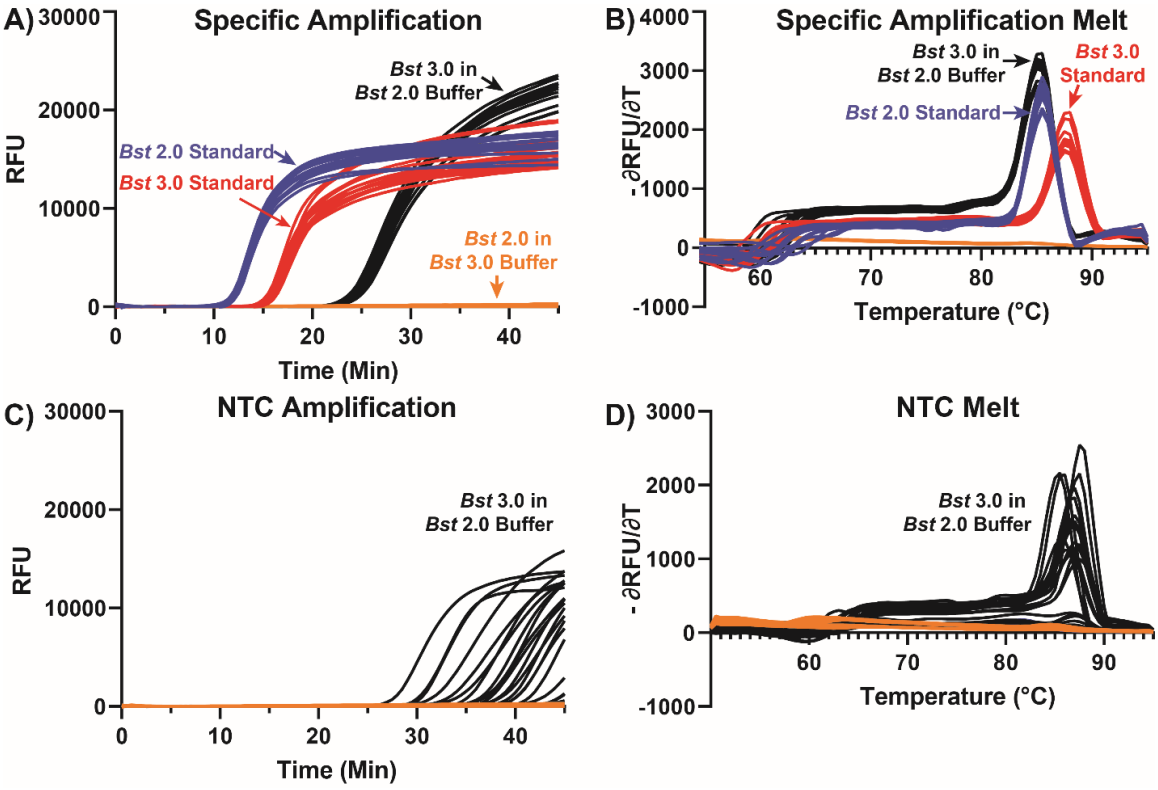

Figure 1.11: Amplification and melting temperature (Tm) curves of *Chlamydia trachomatis* in bulk reactions indicate enzyme sensitivity to varying buffer conditions.

(A-B) Amplification curves in the presence of template (A) and Tm curves (B). (C-D) Nonspecific amplification curves in the no-template control (NTC) (C) and the associated Tm curves (D).

Table 1-1: Summary table of LAMP time to positive (TTP) and product melting temperature (Tm) of *Chlamydia trachomatis* amplicons under a range of buffer conditions.

Condition	Sample	TTP (Min)	Tm (°C)	Amplifications
+ Control	*Bst* 2.0, Standard (7mM Mg^{2+})	12.71±0.23	85.50±0.00	12/12
+ Control	*Bst* 3.0, Standard (8mM Mg^{2+})	16.33±0.30	87.58±0.19	12/12
+ Control, NTC	*Bst* 3.0, Standard (8mM Mg^{2+}), NTC	37.84±1.59	91.00±0.20	44/45
Switch Buffers	*Bst* 2.0, *Bst* 3.0 Buffer	N/A	N/A	0/24
Switch Buffers	*Bst* 3.0, *Bst* 2.0 Buffer	24.95±0.41	85.08±0.19	12/12
Switch Buffers, NTC	*Bst* 2.0, *Bst* 3.0 Buffer; NTC	N/A	N/A	0/24
Switch Buffers, NTC	*Bst* 3.0, *Bst* 2.0 Buffer; NTC	30.75±7.62	86.85±0.72	20/24

We next wished to determine if the behavior associated with nonspecific amplification was inherent to the polymerase or the buffer for both *Bst* polymerases. Buffer composition may influence nonspecific amplification more than the selection of polymerase. We conducted bulk reactions in the presence and absence of template using the standard buffer compositions (Materials and Methods) and the same reactions with each polymerase in the opposite buffer. When we used *Bst* 2.0 polymerase with the *Bst* 3.0 buffer, amplification failed to occur in both the presence and absence of template. When we used *Bst* 3.0 polymerase with *Bst* 2.0 buffer, we observed (i) an 8.6 min delay in TTP (from 16.33±0.30 min to 24.95±0.41 min) in the presence of template (ii) earlier nonspecific amplification in the absence of template, and (iii) greater variation in TTP (from 37.84±1.59 min to 30.75±7.62 min). From these data, we concluded that the difference in nonspecific amplification between conditions was an issue inherent to polymerase selection.

We next tested if the differences in Tm of the target amplicons were due to buffer components. We observed similar sequencing results for these products, but differing Tm. We conducted bulk reactions in the presence of template using the standard buffer composition (Materials and Methods) and the same reactions with each polymerase in the opposite buffer. When all buffer components were switched between the polymerases, *Bst* 2.0 failed to amplify, whereas *Bst* 3.0 resulted in amplicons with Tm similar to *Bst* 2.0 in standard conditions (85.08±0.19 °C). We concluded the *Bst* polymerase produced similar specific products and differences in Tm were due to differences in buffer conditions.

Table 1-2: List of abbreviations used in Figure 1.2, Figure 1.4.

Abbreviation	Long Form
BIP	Backward Inner Primer
rcBIP	Reverse Compliment of BIP
prcBIP	Partial Reverse Compliment of BIP
FIP	Forward Inner Primer
rcFIP	Reverse Compliment of FIP
pFIP	Partial FIP
loopB2	Backward Loop Primer
rcloopb2	Reverse Compliment of Backward Loop Primer
TargetDNA	CT Target DNA sequence
rcTargetDNA	Reverse Compliment CT Target DNA sequence
Rand	Random Insert

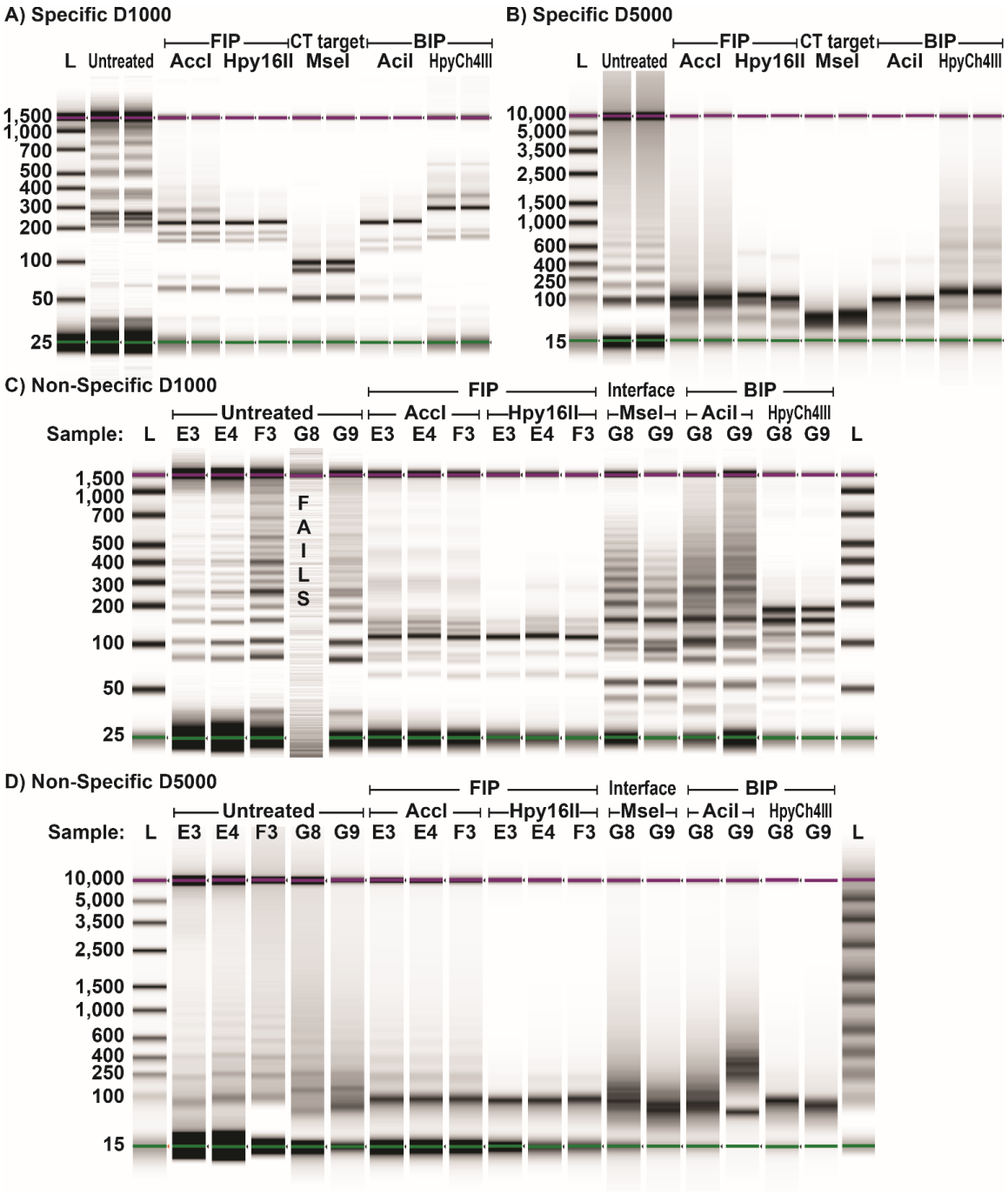

Figure 1.12: Composite images of restriction digestion of *Chlamydia trachomatis* (CT) bulk amplification products.

Digestion of specific amplification products using a D1000 DNA ScreenTape (A) and a D5000 DNA ScreenTape (B). Digestion of nonspecific amplification products using a D1000 DNA ScreenTape (C) and a D5000 DNA ScreenTape (D). AccI and

Hpy16II target restriction site in FIP, MseI in the specific products targets a region within the CT sequences, and in the presence of nonspecific amplification products targets the interface (synthesis across a discontinuous junction) of FIP and BIP. AciI and HpyCh4III target restriction endonuclease sites within BIP.

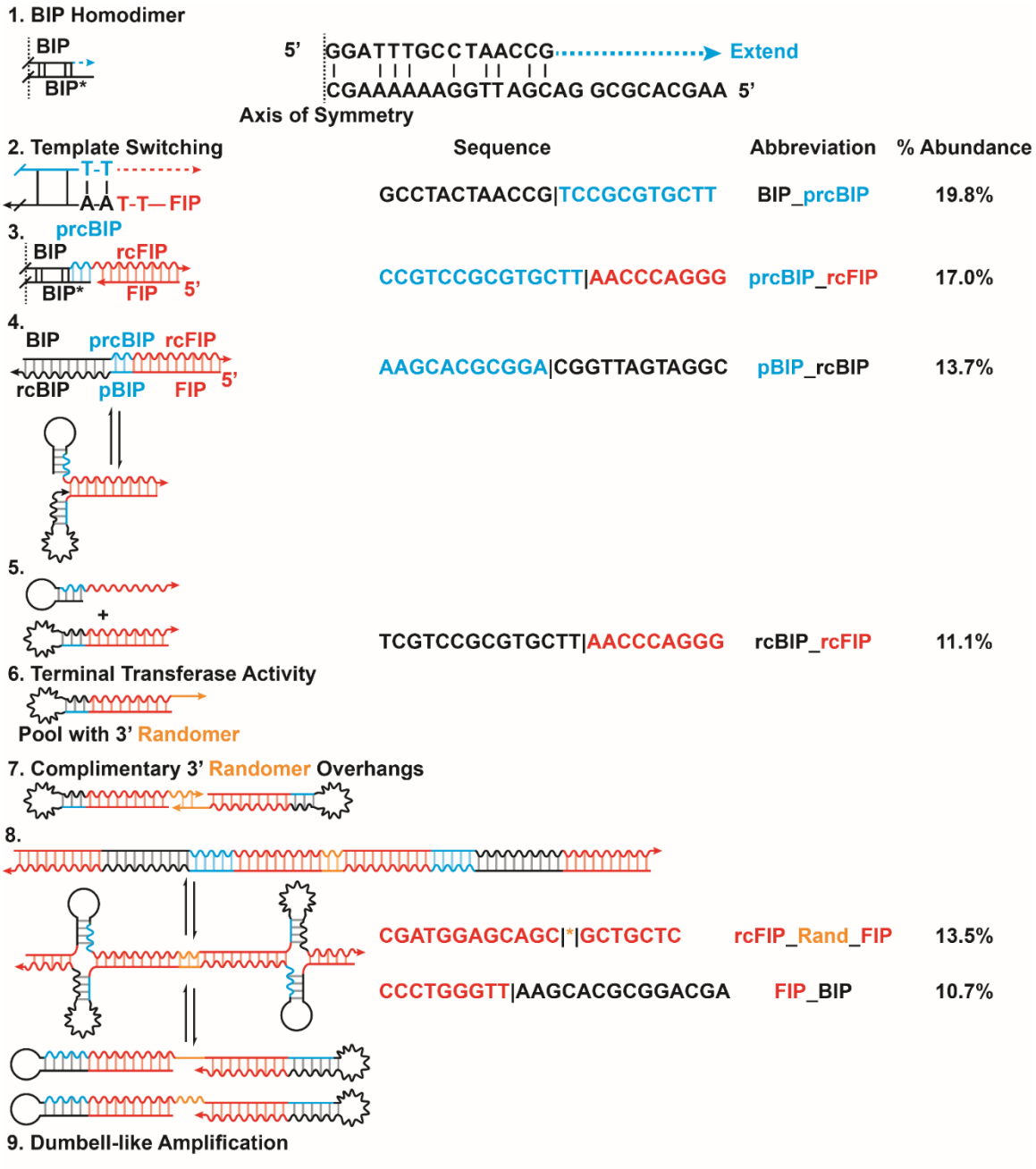

Figure 1.13: Illustration of a simplified mechanism for nonspecific amplification products in LAMP reactions.

Structures and intermediates are labeled with numbers. Percentage abundance reported from **Figure 1.2, Sample E2**.

Bulk and dLAMP reactions with modified primer sets

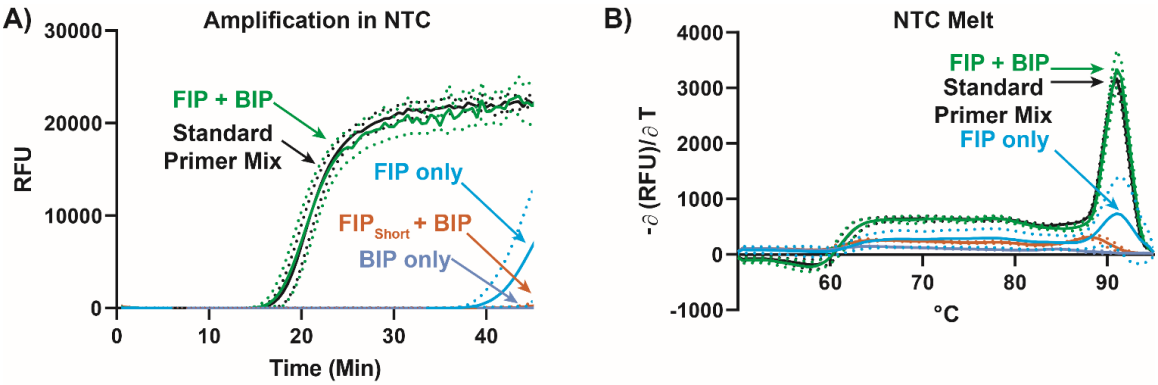

Figure 1.14: Amplification and melting temperature (Tm) curves of *Chlamydia trachomatis* (CT) in a bulk reaction using multiple primer sets show reduced nonspecific amplification upon elimination of primer microhomology.

Plots of average fluorescence as a function of time during the LAMP reaction in the NTC (A) and the corresponding derivative plot of fluorescence as a function of temperature (B). N per condition = 12.

Table 1-3: Time to mean positive and Tm in bulk reactions using multiple primer sets.

N per condition = 12.

Sample	Time to Positive (Min)	Tm (°C)
FIP only	42.3±1.8	91.7±0.8
BIP only	n/a	n/a
FIP + BIP only (No Other Primers)	18.1±1.1	91.0±0.1
Standard Primer Mix	18.3±0.7	91.0±0.0
FIP_{Short} + BIP	n/a	n/a

We analyzed multiple primer sets (**Table S3**) to determine if the nonspecific amplification species produced in the NTC were indeed produced from a combination of primers, as described by the sequencing data in **Figure 1.2** and the mechanism proposed in **Figure 1.4.**

We also wished to test whether nonspecific amplification could occur by single primers, as is known to occur. We conducted bulk reactions in the absence of template using *Bst* 3.0 and the standard primer mixture, FIP and BIP in combination, and the Inner Primers alone and compared the TTP and Tm of these mixtures. The standard primer mixture (consisting of Inner, Outer, and Loop primers) had nonspecific amplification at 18.3±0.7 min with uniform Tm of 91.0±0.0 °C. When the Outer and Loop primers were removed, leaving only FIP and BIP, the mixture amplified with similar TTP and Tm (18.1±1.1 min and 91.0±0.1 °C, respectively) as the standard mixture. In contrast, using BIP alone failed to amplify within 45 min, and FIP alone amplified much later (42.3±1.8 min) and with different Tm (91.7±0.8) than FIP and BIP together or the standard primer mixture. We thus concluded that both FIP and BIP were required to generate the nonspecific products we observed.

The mechanism proposed in **Figure 1.4** requires an interaction between BIP and FIP via microhomology of the 3' of FIP. To confirm the suspected interaction between FIP and BIP, we removed two bases from the 3' end of the FIP primer (hereafter FIP_{Short}). In bulk reactions using FIP_{Short} and BIP with *Bst* 3.0 in the absence of template, we did not observe nonspecific amplification within 45 min. Consequently, we concluded, some of the nonspecific amplification was due to an interaction of the 3' of FIP with BIP.

We next ran the modified primer set in digital LAMP using *Bst* 3.0 to improve our understanding of what occurs at the single-molecule level when primer microhomology is eliminated. We ran three chips in the presence of template and three chips in the absence of template, using the standard primer set (**Figure 1.14A**), and compared the results to the same experiments run with a primer set with FIP_{Short} (**Figure 1.14B**). We observed a significant increase in the percentage of copies detected when using FIP_{Short} (**Figure 1.14C**) using a two-tailed paired t-test ($P = 0.002$), without a difference in TTP (**Table 1-3**). The use of FIP_{Short} did not significantly impact nonspecific amplification products with low Tm in any pairwise ANOVA comparison (**Figure 1.14D,E**). However, we observed a 10-100 fold decrease in nonspecific products with high Tm (**Figure 1.14F, G**). In the absence of template, nonspecific amplification was reduced (**Figure 1.14E**); whereas in the presence of template,

the number of nonspecific amplification products with high Tm was significantly lower at all time points (**Figure 1.14G**).

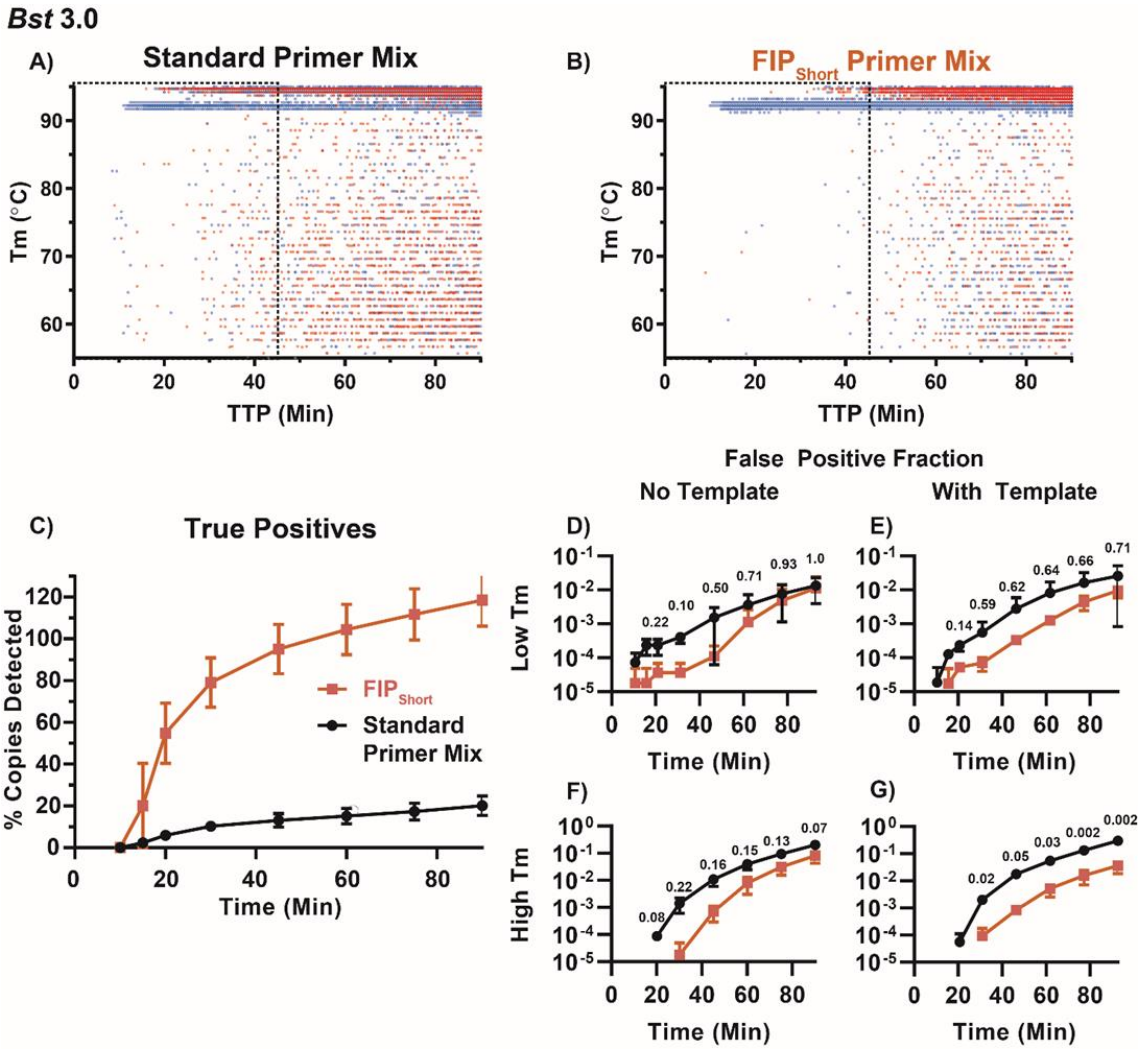

Figure 1.15: Digital, single-molecule plots of specific and nonspecific amplification for multiple primer sets of *Chlamydia trachomatis* show significantly reduced nonspecific amplification with high melting temperature (Tm) upon elimination of primer microhomology.

(A-B) Individual amplification events using *Bst* 3.0 and a primer mixture where FIP is replaced with FIP_{Short} (A) and the standard primer mixture (B). Blue indicates

amplification events in the presence of template; red indicates amplification in the absence of template (NTC). A box is placed around events that occur within 45 min, corresponding to the bulk amplification time. Partitions are rendered at 50% opacity. (C) Plot of the percentage of copies detected (specific amplification) as a function of time. (D-E) The fraction of partitions with nonspecific amplification with Tm less than the specific amplification as a function of time in the absence of template (D) and in the presence of template (E). (F-G) The fraction of partitions with nonspecific amplification with Tm greater than the specific amplification in the NTC as a function of time (F) and in the presence of template (G). Within panels D-G, pairwise *P*-values by t-test are written above each time point.

Table 1-4: Digital, single-molecule comparison of specific and nonspecific amplification for multiple primer sets of *Chlamydia trachomatis* using *Bst* 3.0.

	Time to mode positive (min)
Standard Primer (Set 1)	15.7±2.7
(Set 2)	13.7±0.9
Modified Primer	15.0±1.7

The decrease in nonspecific products with high Tm, upon elimination of the microhomology between FIP and BIP, is consistent with the formation of a nonspecific product predicted by the proposed mechanism in **Figure 1.4**. However, the continued existence of nonspecific products indicates it is possible to form a variety of nonspecific products. Our results indicate that nonspecific products with high-Tm occur even with further primer optimization. The formation of products with high Tm is consistent with our proposed mechanism of branched, mesh-like network. Further investigation should determine if this problem is ubiquitous, even in optimized systems. Additionally, the delay in nonspecific amplification in digital could explain why we did not observe these products in bulk (and thus cannot sequence them).

We believe the mechanism described in **Figure 1.4** is potentially applicable to other primer sets. Amplification observed by FIP alone may follow a similar amplification scheme to **Figure 1.4** via homo-dimerization (**Figure 1.16A**), non-templated synthesis, hairpin dimerization (**Figure 1.16B**), and eventually dumbbell-like amplification (**Figure 1.16D,E**). We observe products consistent with these structures in some of the sequencing data (e.g. **Figure 1.2, Well E1**, which contains elevated rcFIP_pFIP and rcpFIP_FIP).

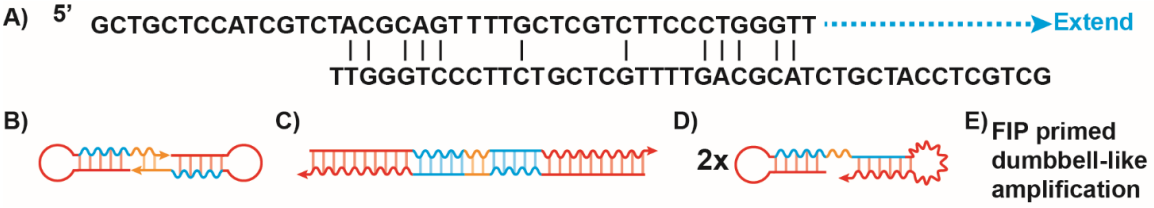

Figure 1.16: Illustration of a mechanism for amplification of FIP alone.
After 3' extension of a FIP homodimer (A), random nucleotides may be incorporated (orange) resulting in self-complimentary hairpins (B). The extension of these hairpins products produce (C): top strand, FIP-prcFIP-rand-pFIP-rcFIP. Upon melting, two self-amplifying dumbbell structures can be produced (D), and undergo further LAMP-like amplification primed by FIP (E).

Table 1-5: Table group of NGS of Randomer inserts within Bulk Sample E1.

E1	
Length	**Percent**
4	53.1
2	41.0
3	2.6
5	1.8
6	1.1

E1: Length n=4	
Sequence	**Percent**
CGTT	38.6
AACG	33.1
AGTT	8.1
AACT	7.5
GGTT	2.5
AACC	2.5
CGTC	1.4
GACG	1.2

E1: Length n=2	
Sequence	**Percent**
AT	28.4
GT	15
AC	13.8
CC	10.3
GG	10.2
CT	9.1
AG	8.3
GC	3.8

Table 1-6: Table group of NGS of Randomer inserts within Bulk Sample E2.

E2	
Length	Percent
3	53.4
11	13.8
4	12.7
2	9.0
5	3.7
8	2.9
14	1.7

E2: Length n=3	
Sequence	Percent
CGT	17.9
ACG	16.5
ACT	12.6
AGT	12.4
ACC	7.2
GGT	6.5
CCC	6.1
GGG	5.3

E2: Length n=11	
Sequence	Percent
AGCAGCAGCAG	20.2
CTGCTGCTGCT	18.9
ATGCTGCTGCT	19.7
AGCAGCAGCAT	18.4
AGCAGCAGCAC	4.7
GTGCTGCTGCT	4.6

Table 1-7: Table group of NGS of Randomer inserts within Bulk Sample F1.

F1	
Length	Percent
5	47.9
3	32.1
4	16.6
2	2.4

F1: Length n=5	
Sequence	Percent
GTTGT	17.8
ACAAC	16.3
GTTGC	15.3
GCAAC	13.4
ATTGC	8.4
GCAAT	8.4
ATTGT	7.7
ACAAT	7.2

F1: Length n=3	
Sequence	Percent
CGT	14.8
ACG	13.7
CGC	13.7
GCG	12.3
AGC	8.9
GCT	8.3
ACT	8.3
AGT	8.3

Does removing outliers impact the distribution of maximum rates?

Occasionally, we observed outlier data points in maximum rate. We asked what caused one point (green circle, max rate 56 RFU, **Figure 1.12A**) to separate from the majority of the data (17 to 30 RFU/30 sec), if these points were common, and if these points were likely to misrepresent the max rate data. We determined the individual trace corresponding to the

outlier amplification event (green trace, **Figure 1.12B**) and observed that the maximum rate for this partition was at 52.5 min, corresponding to a fluctuation in the plateau phase of amplification (dotted line).

We hypothesized that the maximum rate should occur at the observed initial moment of exponential amplification, often slightly before the fluorescence TTP threshold (250 RFU) is reached. To test this hypothesis, we determined the frame (2 per minute) where the amplification trace reached the TTP. From this frame, we subtracted the frame where maximum rate was calculated and plot it against maximum rate (**Figure 1.12C**). Values greater than zero represent partitions where the frame the maximum rate occurs before the fame of TTP, while negative values occur when fame the max rate occurs is after the frame of TTP. We draw a vertical line separating partitions that occur more than 15 min after the TTP (left), from all other partitions.

For the case of *Bst* 2.0, we observed that the mode max rate occurred before the fluorescence TTP by 1 frame (30 sec). Of the 9099 partitions exceeding the 250 RFU threshold, 821 (9.02%) were more than 15 min after the TTP. We expect these partitions to have max rate within the noise of the plateau phase.

A similar trend was observed for *Bst* 3.0 (**Figure 1.12D**). With *Bst* 3.0, the mode max rate occurred 2 frames before the fluorescence TTP (1 min). This value is later than *Bst* 2.0 and is consistent with a slower max rate for *Bst* 3.0 than for *Bst* 2.0. Of the 24,466 partitions reaching the 250 RFU threshold, 1113 (4.55%) were more than 15 min after TTP.

To determine whether removing the partitions with max rate more than 15 min after the TTP impacted the distribution of enzymatic rates, we plotted the fractional cumulative distribution function (CDF) of max rate for all partitions (blue), and the same fractional CDF removing those points more than 15 min after the fluorescence intensity based TTP (red) for *Bst* 2.0 (**Figure 1.12E**) and *Bst* 3.0 (**Figure 1.12F**). Performing a non-parametric based Kolmogorov–Smirnov test to compare the exclusion of partitions with late max rate indicated non-significance between the two CDFs (*Bst* 2.0 P=0.3255, and *Bst* 3.0 $P = 0.1236$). Thus,

we concluded removing late max rate data from the distributions did not impact the CDFs, and therefore does not significantly impact the integrity of our data reporting.

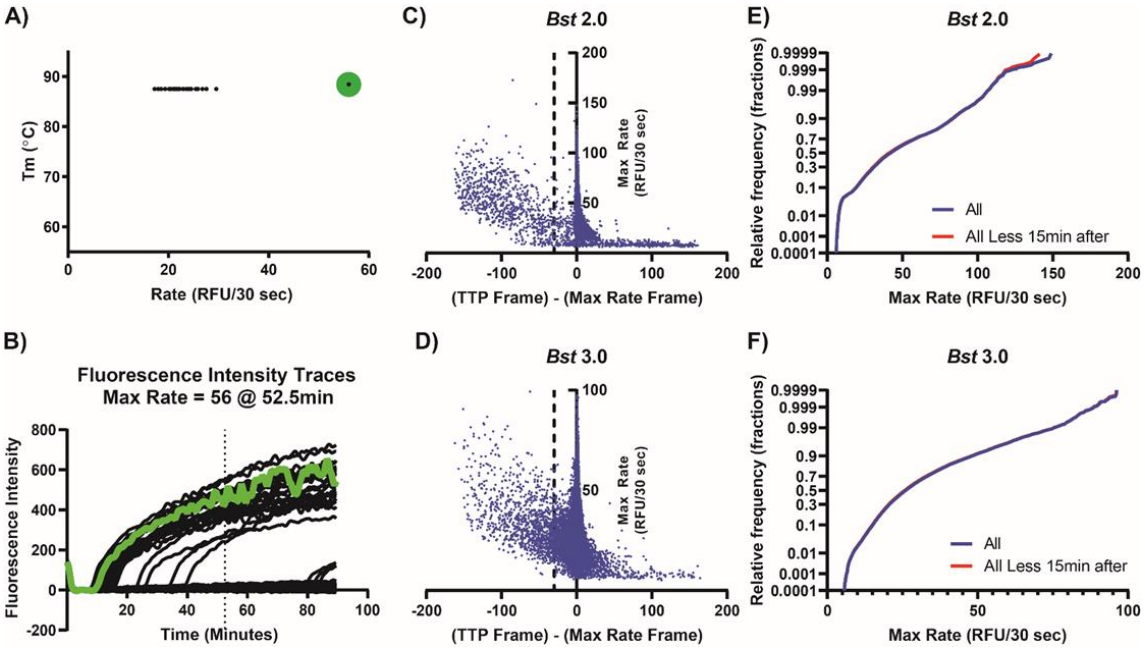

Figure 1.17: Removing outlier data in max rate does not significantly impact summary data.

Plot of observed melting temperature (Tm) as a function of maximum rate, with a possible outlier point highlighted in green (A). Fluorescence traces of individual partition amplification events, with the possible outlier partition's trace highlighted in green (B). The maximum rate for the green trace occurred at 52.5 min (dotted line), corresponding to a fluctuation in the plateau phase of amplification. Plot of maximum rate as a function of the difference between the TTP and max rate frames using *Bst* 2.0 (C) and *Bst* 3.0 (D). Partitions lower than the dashed vertical line represent partitions whose max rate occurred more than 15 min after the TTP frame. Fractional Cumulative Distribution Plots of maximum rate for *Bst* 2.0 (E) and *Bst* 3.0 (f), where the CDF includes all possible partitions (blue), and the same fractional CDF

removing those points more than 15 min after the Fluorescence Intensity based TTP (red).

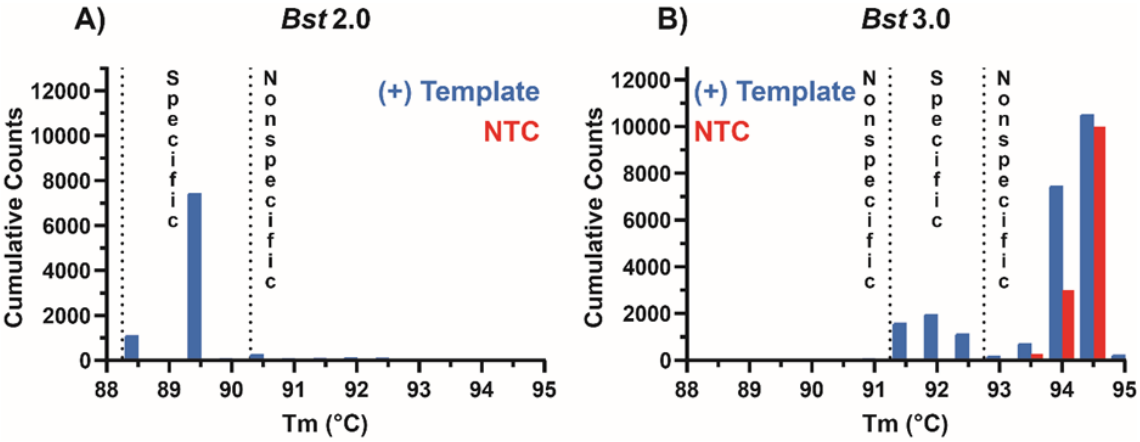

Figure 1.18: Histogram plots of Tm after 90 min of digital LAMP targeting CT in the presence of template (blue) and NTC (red) can be used to distinguish specific from nonspecific amplification.

Tm of amplification using *Bst* 2.0 (A) and *Bst* 3.0 (B). Dashed lines indicates the upper and lower bounds used for separating specific and nonspecific amplification. *Bst* 2.0: 88.5-90.3°C, *Bst* 3.0: 91.25-92.75 °C. Bin width in both graphs 0.5 °C, with the (+) template left of the tick and NTC right of the tick. NTC is illustrated with red bars, and the presence of template with blue bars.

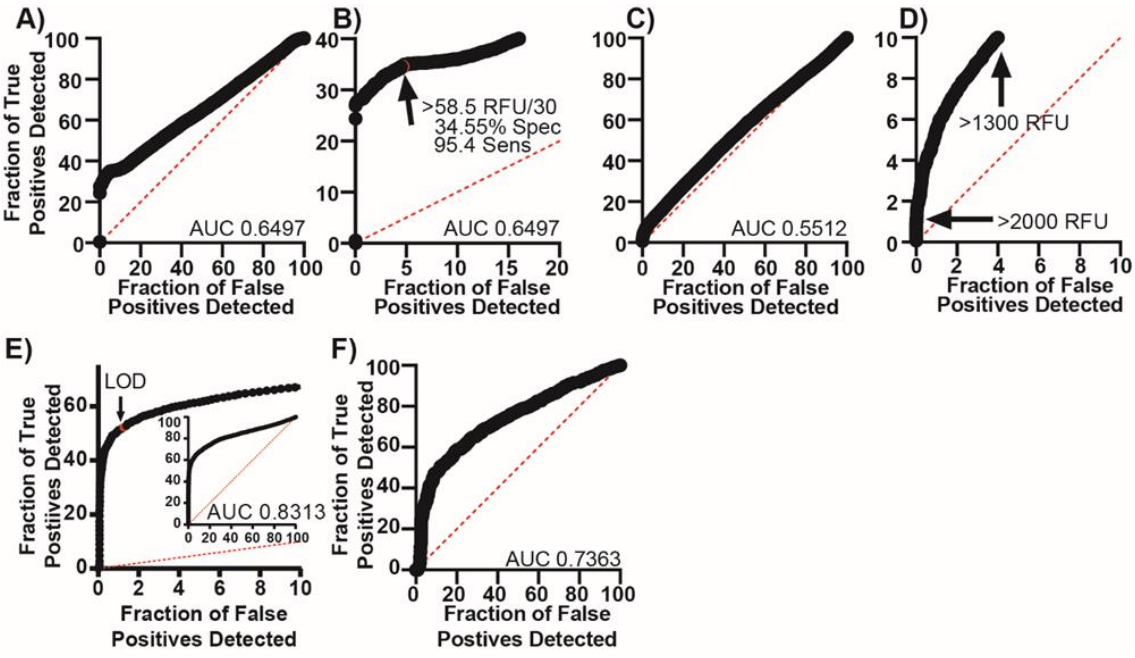

Figure 1.19: Receiver operating characteristic (ROC) curves using HRM to determine optimal performance of dLAMP assays.

(A) ROC curve using *Bst* 3.0, plotting the fraction of true positives detected versus the fraction of false positives detected using a threshold on max rate. (B) ROC curve using *Bst* 3.0, plotting the fraction of true positives detected less than 40% versus the fraction of false positives detected less than 20% using a threshold on maximum rate. Arrow indicates corresponding LOD. (C) ROC curve using *Bst* 3.0, plotting the fraction of true positives detected versus the fraction of false positives detected using a threshold on final intensity of the partition. (D) ROC curve using *Bst* 3.0, plotting the fraction of true positives detected less than 10% versus the fraction of false positives detected less than 10% using a threshold on final intensity of the partition. Arrows indicate final-intensity thresholds of >2000 RFU and >1300 RFU. (E) ROC curve using *Bst* 3.0, plotting the fraction of true positives detected versus the fraction of false positives detected using a threshold on TTP. Arrow indicates LOD. (F) ROC curve using *Bst* 2.0, plotting the fractions of true versus false positives detected using a threshold on TTP.

Summary Data of Mode TTP

Table 1-8: Time to mode positive in minutes.

N=3 chips per set. Human Haploid Genome Equivalents (HHGE) are per microliter.

HHGE per µL	0	0.01	1	100	5000
Bst 2.0	11.8 ± 0.2	11.7±0.2	11.3±0.2	11.7±0.6	16.3±2.7
Bst 3.0 (Set 1)	15.7± 2.7	13.8±1.2	18.2 ±4.4	14.7± 1.7	
(Set 2)	13.7± 0.9			17.2± 2.1	17.2± 2.1

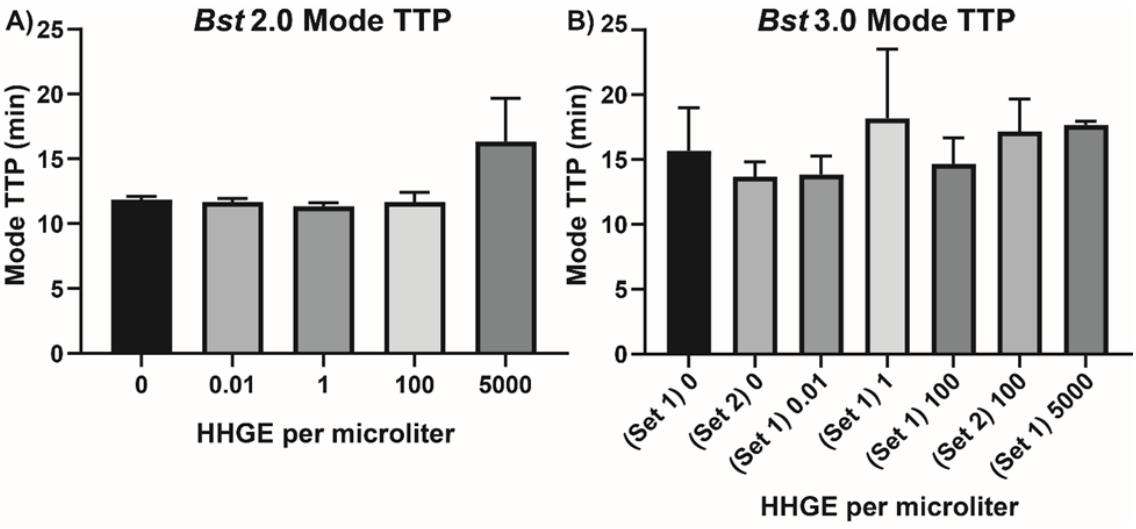

Figure 1.20: Time to mode positive for *Bst* 2.0 (A) and *Bst* 3.0 (B) under variable concentrations of host human genomic DNA (hgDNA).

Human Haploid Genome Equivalents (HHGE) are per microliter.

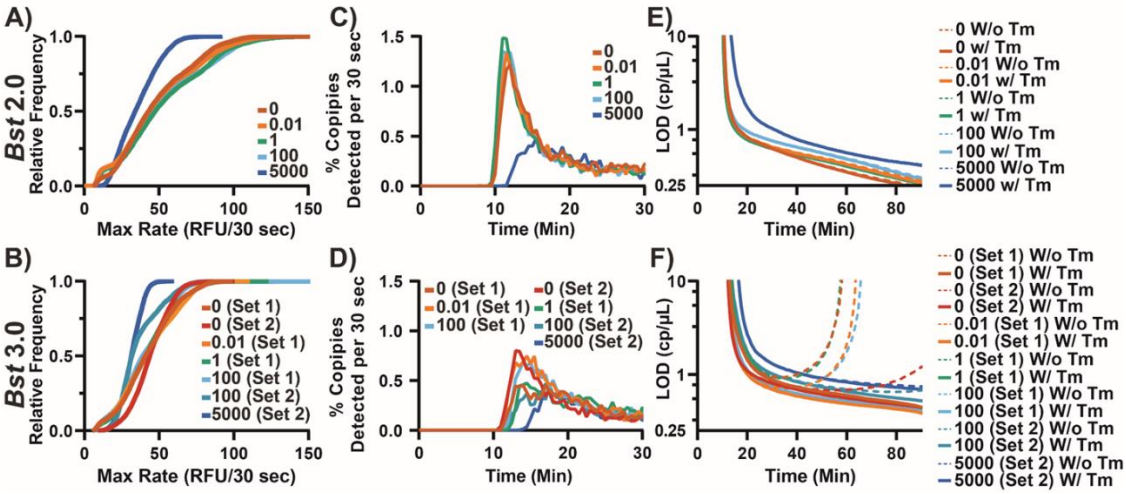

Figure 1.21: Evaluation of the impact of gDNA on assay performance.

Fractional cumulative distribution function (CDF) of maximum rates of amplification using *Bst* 2.0. (A) and *Bst* 3.0 (B) CDFs are plotted as the sum of replicates. Distribution plot of time to fluorescence threshold for *Bst* 2.0 (C) and *Bst* 3.0 (D) using arithmetic mean. LOD as a function of time using *Bst* 2.0. (E) and *Bst* 3.0 (F).

Table 1-9: Tabular form of % copies detected from Figure 1.9 using *Bst* 2.0.

Time (Min)	0 HHGE per µL	0.01 HHGE per µL	1 HHGE per µL	100 HHGE per µL	5000 HHGE per µL
10	0.01±0.02	0.00±0.00	0.04±0.03	0.02±0.02	0.00±0.00
15	8.21±0.72	8.35±0.56	9.42±0.56	8.98±0.81	1.67±2.32
20	11.92±0.35	12.04±0.20	12.86±0.54	12.34±1.44	5.24±3.69
30	15.94±1.13	15.41±0.36	16.15±0.66	15.65±1.98	9.19±2.66
45	22.20±4.37	19.30±0.85	20.16±1.12	19.84±1.73	13.42±1.99
60	28.88±8.07	23.68±2.49	24.94±3.05	25.00±1.11	16.96±2.03
75	36.10±11.86	29.93±5.30	31.24±5.83	31.81±2.83	20.34±2.17
90	43.77±14.98	37.47±8.62	38.47±10.05	40.69±5.32	23.12±2.35

Table 1-10: Tabular form of % copies detected from Figure 1.10 using *Bst* 3.0.

Time (Minutes)	0 HHGE per µL (Set 1)	0 HHGE per µL (Set 2)	0.01 HHGE per µL (Set 1)	1 HHGE per µL (Set 1)	100 HHGE per µL (Set 1)	100 HHGE per µL (Set 2)	5000 HHGE per µL (Set 2)
10	0.00±0.00	0.00±0.00	0.00±0.01	0.00±0.00	0.00±0.00	0.00±0.00	0.00±0.00
15	2.28±1.99	4.13±0.98	3.83±2.47	1.71±1.54	2.86±1.04	1.37±1.89	0.05±0.08
20	5.96±2.47	8.15±0.31	8.93±2.44	5.21±4.50	7.89±0.66	4.81±2.04	3.04±0.93
30	10.19±2.48	11.23±0.23	13.33±1.84	10.26±3.32	12.41±0.24	8.82±1.06	6.86±1.05
45	13.02±3.28	14.07±0.80	16.74±1.87	13.92±2.80	15.67±0.38	11.60±1.12	9.35±1.09
60	15.09±3.68	16.28±1.71	19.13±1.83	16.37±2.69	17.89±0.29	13.81±1.70	10.92±1.38
75	17.25±4.02	18.38±3.13	21.00±2.20	18.61±3.05	19.95±0.45	15.62±2.34	12.11±1.16
90	20.11±4.71	20.44±4.50	23.97±3.58	21.13±3.99	23.00±0.87	17.37±3.16	13.10±1.81

Caption for 4D videos

Videos plot the TTP, max rate, final intensity, and Tm data of both specific and nonspecific amplification reactions using either *Bst* 2.0 (Video 1) and using *Bst* 3.0 (Video 2). Time to positive (TTP), max rate, and melting temperature (Tm) are plotted on the axes; final intensity is indicated by the color of each data point (scale provided in **Figure 1.6Q-R**).